A Turnkey Data Logger Program for Field-Scale Energy Flux Density Measurements Using Eddy Covariance and Surface Renewal

Thomas M. Shapland [1], Andrew J. McElrone [1,2], Khaw Tha Paw U [3], Richard L. Snyder [3]*

Abstract: *Micrometeorological methods and ecosystem-scale energy and mass flux density measurements have become increasingly important in soil, agricultural, and environmental sciences. For many scientists without formal training in atmospheric science, these techniques are relatively inaccessible. Eddy covariance, surface renewal, and other flux measurement methods require an understanding of boundary layer meteorology and extensive training in instrumentation and multiple data processing programs. In this paper, we present an open-source turnkey data logger program that performs flux data acquisition and post-processing, returning to the user a simple data table with the corrected energy balance fluxes and quality control parameters. The underlying theory of the flux measurements is briefly discussed and the program design and execution are described line by line. Data were collected over a wheat canopy and the program results were tested against other flux processing software, including EdiRe and R. The energy balance fluxes appear reasonable for the fair weather conditions found during data collection period. The daily cumulative evapotranspiration values from the flux tower and logger program show strong agreement with measurements from a precision weighing lysimeter. The logger program can be accessed at sites.google.com/site/tmshapland.*
Keywords: *atmospheric surface-layer fluxes, energy balance, evapotranspiration, latent heat flux density, lysimetry, micrometeorology.*

Riassunto: *I metodi micro-meteorologici e le misure dei flussi di massa e di energia alla scala di ecosistema hanno recentemente acquisito importanza nelle scienze agrarie, del suolo e dell'ambiente. Queste tecniche sono relativamente inaccessibili ai molti ricercatori che non abbiano una preparazione tecnica in meteorologia. Eddy covariance, surface renewal e altri metodi per la misura dei flussi richiedono familiarita' con i fondamenti della meteorologia dello strato di confine atmosferico ed una profonda conoscenza della strumentazione e dei programma di analisi dei dati. In questo articolo presentiamo un programma open source pronto all'uso per l'acquisizione e l'analisi di dati, che fornisce come risultato una semplice tabella con i flussi di energia corretti ed i parametri di controllo dei dati. La teoria alla base delle misurazioni è brevemente discussa e la struttura e l'esecuzione del programma sono descritte linea per linea. I dati sono stati acquisiti su una coltura di frumento ed i risultati del programma sono stati validati in comparazione con altri programmi di analisi di dati di flusso, fra cui EdiRe e R. I flussi del bilancio energetico appaiono ragionevoli per le condizioni di bel tempo del periodo di raccolta dati. I valori cumulati giornalieri di evapotraspirazione, provenienti dalla torre di misura dei flussi e dal datalogger, mostrano un'ottima corripondenza con i dati misurati da un lisimetro a pesata di precisione. Il programma per datalogger può essere scaricato dal sito: sites.google.com/site/tmshapland.*
Parole chiave: *flussi atmosferici nello strato di confine, bilancio energetico, evapotraspirazione, flusso di calore latente, micrometeorologia, sistemi di misura online.*

1. INTRODUCTION

The measurement of ecosystem-scale energy and mass flux densities is important in the study of agrometeorology, especially as climate change, environmental policy, and growing urban demands limit agricultural water resources (e.g., California Department of Water Resources, 2005). Agrometeorologists measure evapotranspiration (*ET*) to evaluate experimental treatments for improving crop water use efficiency (e.g., Moratiel and Martinez-Cob, 2011), to provide growers with crop coefficient information (Doorenbos and Pruitt, 1977), and to parameterize regional water allocation strategies (Snyder *et al.*, 2005). Evapotranspiration measurements also have the potential to empower growers with site-specific crop water demand and irrigation management information. Eddy covariance (Swinbank, 1951) and surface renewal (Paw U *et al.*, 1995) are two methods for measuring turbulent fluxes such as sensible heat flux density (*H*).

* Corresponding author.
R.L. Snyder e-mail: rlsnyder@ucdavis.edu
[1] Department of Viticulture & Enology, University of California, Davis, CA, U.S.A.
[2] United States Department of Agriculture-Agricultural Research Service, Crops Pathology and Genetics Research Unit, Davis, CA, U.S.A.
[3] Atmospheric Science, University of California, Davis, CA, U.S.A.
Received 7 August 2012, accepted 29 November 2012.

When H measurements are taken in conjunction with net radiation (Rn) and ground heat flux density (G) measurements or estimates, latent heat flux density (λE) can be calculated from the energy balance residual, providing an inexpensive approach to estimate ET.

The successful deployment of an eddy covariance flux tower for ET measurements can be a daunting challenge, especially for many agricultural researchers without formal training in atmospheric science. Eddy covariance and surface renewal measurements require sophisticated technical skills in both programming data loggers to execute tasks with complex instrumentation and writing computer programs to post-process the raw turbulence data into meaningful fluxes. Furthermore, because high-frequency measurements are needed for both eddy covariance and surface renewal, agrometeorologists face the additional challenge of managing vast amounts of data. Even for experienced agrometeorologists with theoretical and practical expertise in ecosystem-scale flux measurements, data management and post-processing are tedious and time-consuming endeavors.

We have developed a turnkey data logger program for ET measurements that streamlines the data collection and post-processing procedures, facilitating access to micrometeorology for neophytes and adding convenience for experienced flux scientists. The program collects and stores raw data from the Rn, G, and H sensors. The raw data are processed in the logger program, appropriate corrections are applied, and the corrected fluxes, including λE from the energy balance residual, are output on a simple and convenient data table. In this paper we summarize the theoretical basis of the flux calculations, describe the design and execution of the program, and validate the program against other flux processing software using data collected over a wheat canopy. The logger program results agree well with lysimeter measurements and with the expected course of diurnal energy balance fluxes during fair weather conditions.

2. EXPERIMENTAL DATA, INSTRUMENTATION, AND ANALYSIS

The program was installed in a CR1000 data logger (Campbell Scientific Inc., Logan, UT, U.S.A.) and tested over a wheat canopy from February 14 2012 to June 12 2012 at the Campbell Tract at the University of California, Davis (38°32'N, 121°46'W). The data presented in this paper are from five contiguous days, April 19 2012 to April 23 2012 (Day of year 111 to 115), when the meteorological conditions were typical for the region and season, i.e., clear and sunny, allowing for a detailed comparison of the expected energy balance fluxes and the output of the logger program. The wheat canopy height was 0.9 m and fetch was 100 m in the prevailing wind direction (south). The three-dimensional wind velocities and sonic temperature were sampled at 10 Hz with a sonic anemometer (81000RE, R.M. Young Company, Traverse City, MO, U.S.A) installed at 1.6 m above the ground (Tab. 1). Note that the sonic anemometer requires reconfiguration from the factory settings prior to field deployment to output the desired signals (For more information, see *RM Young Model 81000RE Reconfiguration Instructions.pdf* available at sites.google.com/site/ tmshapland). The air temperature was also sampled at 10 Hz with a 76 µm diameter fine wire thermocouple (FW3, Campbell Scientific Inc., Logan, UT, U.S.A.) located at 1.35 m above the ground, and net radiation measured with a net radiometer (NR-Lite, Kipp & Zonen B.V., Delft, The Netherlands) at 1.80 m above the ground. Two soil heat flux plates (HFT-3.1, REBS Inc., Seattle, WA, U.S.A.) were buried 0.05 m below the soil surface, and a soil thermocouple (TCAV, Campbell Scientific Inc., Logan, UT, U.S.A.) was installed to span the volume of soil above the heat flux plate and provide temperature change to estimate the surface ground heat flux associated with heat storage above the plates.

Evapotranspiration data were also collected from a 6.1 m diameter weighing lysimeter (Pruitt and Angus, 1960). The flux tower was located approximately 15 m to the west of the lysimeter. The plants inside the lysimeter were slightly less densely spaced and about 10 cm shorter than plants in the surrounding field.

The energy balance terms calculated by the logger program were tested against EdiRe flux processing software (Mauder *et al.*, 2008) and functions written in the R statistical environment (R Development Core Team, 2012).The comparison analysis among software programs and graphics generation were performed in R.

3. FLUX MEASUREMENT THEORY

3.1. Net radiation

Net radiation is the total incoming radiation impinging on the surface minus the total outgoing radiation. Like many net radiometers, the sensor used in this study absorbs short and long waveband radiation on both sides of the sensor. The voltage output depends on the difference between the radiation received from the upper and lower surface of the sensor, and the voltage reading is converted from volts to energy flux density using a calibration factor determined by the manufacturer.

3.2. Ground heat flux density

Ground heat flux density is energy conducted into or out of the ground. It can be measured using a ground

Sensor	Model	Manufacturer	Sensor wire color or port	Data logger channel or port
Air thermocouple	FW3	Campbell Scientific Inc.	Purple	1H
			Red	1L
			Clear	Signal ground
Net radiometer	NR-Lite	Kipp & Zonen B.V.	White	2H
			Green	2L
			Shield (bare)	Signal ground
			Jumper wire	2L to Signal ground
Ground heat flux plate	HFT-3.1	REBS Inc.	Black	3H
			Red	3L
			Shield (bare)	Signal ground
Ground heat flux plate	HFT-3.1	REBS Inc.	Black	4H
			Red	4L
			Shield (bare)	Signal ground
Soil thermocouple	TCAV	Campbell Scientific Inc.	Purple	5H
			Red	5L
			Shield (bare)	Signal ground
Sonic anemometer	81000RE	R.M. Young Company	RX	C7
			TX	C8
			Serial reference	G
			+PWR	12V
			PWR reference	G
			Earth ground	G

Tab. 1 - Instrumentation and wiring diagram.
Tab. 1 - Strumentazione e diagramma di connessione dei cavi.

heat flux plate and soil temperature sensors. The thermopile inside the ground heat flux plate measures the temperature gradient across a material with known thermal properties to arrive at the energy flux density. Each plate is calibrated by the manufacturer. Because ground heat flux plates cannot be placed directly on top of the soil without intercepting solar radiation, they must be buried below the soil surface. The energy flux density at the depth of the ground heat flux plates is not the same at the energy flux density at the surface because some energy is stored in the soil layer above the plate, so a set of soil thermocouples wired in parallel are installed in the layer above the plates. The following continuity equation is used with the heat flux plate output and the change in heat storage within the soil layer above the plates to estimate the ground heat flux G at the surface:

$$G = G' + \Delta S \qquad (1)$$

where G' is the ground heat flux density at the plates and ΔS is the change in heat storage per unit area in the soil layer above the heat flux plates. The latter term is expressed as

$$\Delta S = C_v \left(\frac{T_f - T_i}{t_f - t_i} \right) d_g \qquad (2)$$

where T_f is the final temperature (K) at time t_f and T_i is the initial temperature (K) at time t_i, d_g is the depth (m) from the soil surface to the heat flux plates, and C_v is the volumetric heat capacity (J m^{-3} K^{-1}). Soil volumetric heat capacity can be estimated according to de Vries (1963) and Jensen, Burman, and Allen (1990).

$$C_v = \left(1.93 V_m + 2.51 V_o + 4.19\theta\right) 10^6 \qquad (3)$$

where (V_m) is the volume fractions of minerals, (V_o) is the volume fraction of organic matter, and (Θ) is the volumetric water content. Since V_o is typically small and the soil bulk density (P_b) is related to V_m, one can also estimate C_v using the equation:

$$C_v = \left(0.837 \rho_b + 4.19\theta\right) 10^6 \qquad (4)$$

The factor 10^6 converts the soil and water densities from Mg m^{-3} to g m^{-3}. Multiplying the densities by the apparent specific heats for soil and water, 0.837 (J g^{-1} K^{-1}) and 4.19 (J g^{-1} K^{-1}), respectively, gives C_v in J m^{-3} K^{-1}. In the logger program, the soil bulk density is assigned a default value of 1.3 Mg m^{-3} and the volumetric water content is assigned a default value of 0.2, although the logger program can be modified to include other default values or to make measurements with volumetric water content sensors. The soil heat flux density is usually less than 15% of *Rn*, so small errors in the soil heat flux storage term in the thin soil layer above the plates, caused by differences between the default soil parameters and the actual soil characteristics, should not create large errors in the λE calculation.

3.3. Sensible heat flux density

Sensible heat flux density is the energy flux density from the surface to the air or vice-versa. The logger program calculates *H* using both the eddy covariance and surface renewal techniques.

3.3.1. Eddy covariance

Eddy covariance measures the turbulent fluctuations in vertical wind speed and the air temperature to arrive at *H* (Swinbank, 1951) with the following equation:

$$H = \rho C_p\left(\overline{w'T_s'}\right) \tag{5}$$

where ρ is the air density (g m^{-3}), *Cp* is the specific heat per unit mass of air at constant pressure (J g^{-1} K-1),w, is the vertical wind velocity (m s^{-1})^{Ts}, is the sonic temperature (K), the prime signifies the instantaneous departure from the mean and the overbar denotes a time-averaged interval.

To eliminate a major source of error in eddy covariance measurements, a two-dimensional coordinate rotation correction is applied in the logger to force the mean cross and vertical wind velocities to zero (Tanner and Thurtell, 1969). The rotation angles are calculated as follows:

$$\sin\theta = \frac{\overline{w}}{\sqrt{\overline{u}^2 + \overline{v}^2 + \overline{w}^2}} \tag{6a}$$

$$\cos\theta = \frac{\sqrt{\overline{u}^2 + \overline{v}^2}}{\sqrt{\overline{u}^2 + \overline{v}^2 + \overline{w}^2}} \tag{6b}$$

$$\sin\eta = \frac{\overline{v}}{\sqrt{\overline{u}^2 + \overline{v}^2}} \tag{6c}$$

$$\cos\eta = \frac{\overline{u}}{\sqrt{\overline{u}^2 + \overline{v}^2}} \tag{6d}$$

The trigonometric functions are used to calculate the tilt-corrected sonic temperature flux:

$$\overline{w'T_S'} = \overline{w'T_S'}_{raw}\cos\theta - \overline{u'T'}_{S\,raw}\sin\theta\cos\eta - \overline{v'T'}_{S\,raw}\sin\theta\sin\eta \tag{7}$$

and the tilt-corrected momentum flux density normalized by air density:

$$\overline{u'w'} = \overline{u'w'}_{raw}\cos\eta\left(\cos^2\theta - \sin^2\theta\right) + \overline{v'w'}_{raw}\sin\eta\left(\cos^2\theta - \sin^2\theta\right) + \overline{\left(w'\right)^2}_{raw}\sin\theta\cos\theta - \overline{\left(u'\right)^2}_{raw}\sin\theta\cos\theta\cos^2\eta - \overline{\left(v'\right)^2}_{raw}\sin\theta\cos\theta\sin^2\eta - 2\overline{u'v'}_{raw}\sin\theta\cos\theta\sin\eta\cos\eta \tag{8}$$

3.3.2. Surface renewal

Surface renewal is based on analyzing the energy budget of air parcels, or coherent structures, that reside ephemerally within the crop canopy during the turbulent exchange process (Paw U *et al.*, 1995). The air parcels are manifested as ramp-like shapes in turbulent temperature time series data, and the amplitude and period of the ramps are used to calculate the flux density.

$$H = \alpha z \rho C_p \frac{a}{\tau} \tag{9}$$

where α is the alpha calibration factor, z is the measurement height (m), a is the ramp amplitude (K), and τ is the ramp period (s). Surface renewal flux density measurements are calibrated against an independent flux measurement technique, such as eddy covariance. The alpha calibration is obtained as the slope of the least squares linear regression forced through the origin, and its value depends on sensor height, canopy height, canopy architecture, atmospheric stability, turbulent characteristics, and sensor dynamic response characteristics (Paw U *et al.*, 1995; Paw U *et al.*, 2005). In the logger program, the alpha calibration is assumed to be unity unless the user changes the default value. By setting alpha to a default value of one, the surface renewal values output by the logger program have not been calibrated. Once the calibration has been determined, the user can change the default value of the alpha calibration to the actual alpha calibration.

The Van Atta (1977) procedure is used to resolve the ramp amplitude and ramp period from the air temperature data for the surface renewal calculation (Paw U *et al.*, 1995; Spano *et al.*, 1997). In the first step of the procedure, the structure function is calculated from the high frequency air temperature data.

$$\overline{S^n(r)} = \frac{1}{m-j}\sum_{k=1}^{m-j}\left[\left(T_k - T_{k-j}\right)^n\right] \tag{10}$$

where $\overline{S^n(r)}$ is the n^{th}-order structure function, m is the number of points in the time series, j is the sample lag between points, TK is the element in the scalar time series. The time lag (r) is calculated as the sample lag divided by the sampling frequency ($r = j / f$). The structure function values constitute the coefficients in the following cubic polynomial:

$$0 = a^3 + pa + q \tag{11a}$$

where

$$p = \left[10\overline{S^2(r)} - \frac{s^5(r)}{s^3(r)}\right] \tag{11b}$$

and

$$q = 10S^3(r) \tag{11c}$$

Equation (11a) is solved in the logger program using an analytical solution method to obtain the ramp amplitude. The ramp period is calculated from the ramp amplitude, the structure function time lag, and the third-order structure function, as follows:

$$d + s = -\frac{a^3 r}{S^3 r} \tag{12}$$

Although it is not shown here for the sake of brevity, the analytical solution method fails outside of a narrow range of structure function time lags if the ramp amplitude is negative (i.e., the odd-ordered structure function is positive). For data intervals with positive ramp amplitudes, i.e., during unstable thermal conditions, a broader range of structure function time lags is acceptable than for stable stratification data intervals with negative ramps. In earlier surface renewal studies, this mathematical artifact limited the number of stable thermal intervals that were successfully resolved, introducing uncertainty into flux measurements and requiring gap filling strategies (e.g., Shapland et al. 2012c). Van Atta (1977) demonstrated that the sign of the ramp amplitude in a ramp model time series is always opposite of the odd-ordered structure function. If one artificially reverses the sign of the third- and fifth-ordered structure function values, passes them into the Van Atta procedure, the sign of the ramp amplitude is also reversed. To expand the range of acceptable time lags for data intervals with negative ramps, the logger program converts positive third- and fifth-ordered structure function values into negative values, passes the structure function values into the cubic polynomial, and resolves the magnitude of the ramp amplitude using the analytical solution method. Then, the original sign (negative) of the ramp amplitude is reintroduced, according to the sign of the original third-order structure function.

3.4. Latent heat flux density and evapotranspiration

Latent heat flux density is the energy flux density associated with the water vapor mass flux density between the surface and the atmosphere. The latent energy flux density is obtained in the logger program from the energy balance residual.

$$\lambda E = R_n - G - H \tag{13}$$

The tilt-corrected eddy covariance H is used in the energy balance residual equation because it does not require a calibration factor, unlike the surface renewal H. Latent heat flux density is then divided by the latent heat of evaporation (λ) to obtain the mass flux density of water vapor, i.e., ET.

$$ET = \frac{\lambda E}{\lambda} \tag{14}$$

4. SOFTWARE

The program is written in the Campbell Scientific CRBasic language for the CR1000 data logger, but it can be easily modified for most other modern Campbell Scientific loggers. The program is named “RMYS_2HFP_KZ.CR1”, an abbreviation for RM Young in Serial mode with 2 Heat Flux Plates and a Kipp and Zonen net radiometer. One can adapt the program for other sensor configurations, but the user should carefully field test the logger program after any modifications. If many new lines of complex code are added to the program, then it may not function properly; especially when the sonic anemometer is sampled in serial rather than analog mode. The program is available for download at sites.google.com/site/ tmshapland.

4.1. Program design

When the program is opened with CRBasic or a text editor, the user first sees the notes describing the title of the program, its contributors, its maintainer, instructions for citing the program, and an overview of the program design and functionality (lines 1-48).
The user next encounters the site-specific user inputs (lines 49-69), including the sonic anemometer and thermocouple heights, the net radiometer calibration constants, the heat flux plate calibration constants, the estimated volumetric water content, and the estimated soil bulk density. A note next to each input describes the parameter and its units. The user should enter the appropriate site-specific values in this section. If the

canopy is no longer actively growing and the distance between the sensor and canopy top is no longer changing, then the user can enter the surface renewal alpha calibration. Parameters that are not site-specific, and therefore should not be changed by the user, are declared in the next section (lines 70-91).

The wiring diagram is described in lines 92-147 using the wire colors of sensors distributed in the United States and in Tab. 1. The instructions indicate where to connect the wires from each sensor to the appropriate logger channels and ports. Note that wire colors could vary for different sensors and by country.

Because CRBasic language is a compiled language, rather than interpreted language, all variables must first be declared at the start of the program. The variable declarations are organized such that the high-frequency variables are first (lines 148-181), the structure function and covariance variables are second (lines 182-205), the variables that are used to calculate the turbulent fluxes using the surface renewal and eddy covariance methods are third (lines 206 – 280), the preliminary G and Rn are fourth (lines 281-290), and the energy balance and diagnostic variables are last (lines 291-332).

In the next section, the data tables are declared, including the data table for the raw turbulent signals (turb_raw, lines 338-343), the data table for the preliminary fluxes (preflux, lines 348-367), the data table for the preliminary Rn and G measurements (preRnG, lines 372-381), and the energy balance data table, i.e., the ultimate output of the program (EB, lines 387-412). Next to each term in the EB data table, its meaning is described as a comment. The EB data table terms and their units are also defined in Tab. 2.

4.2. Program execution

The final section of the program, constituting the last third of the lines (425-623), contains the executable commands that instruct the logger on sampling the various instruments and processing the data. The program first samples the high-frequency (10 Hz) turbulent variables, i.e., the three dimensional wind velocities, the sonic temperature, and the thermocouple air temperature. The sonic anemometer is sampled in serial mode (lines 425-439). If the data transfer from the sonic anemometer to the data logger fails during a scan, the character string “NaN” (Not a Number) is recorded, and the logger program is unable to calculate statistics, such as covariance or mean, and hence unable to calculate the energy balance fluxes. To avoid this problem, “NaN” strings are replaced with the values from the previous scan (lines 440-446). The voltage from the reference junction of the thermocouple is sampled and converted to Celsius using the CRBasic thermocouple differential channel function, and the second-, third-, and fifth-order structure function values at a 0.5 time lag are calculated from the sonic temperature and the thermocouple air temperature measurements (lines 447-461). Because the reference temperature used for thermocouple readings in Campbell Scientific data loggers is the panel temperature, which changes slowly, and only the high frequency thermocouple temperature fluctuations are used in surface renewal measurements, environmental shielding of the data logger is not critical, unlike the requirements for making slow-response absolute temperatures measurements. The structure function values are the input statistics for resolving the sonic temperature and air temperature ramp characteristics (Van Atta, 1977) that are used to calculate the surface renewal H (Paw U *et al.*, 1995; Spano *et al.*, 1997). The CallTable commands tell the logger to store the high-frequency turbulent signals in the turb_raw data table (line 462) and calculate the structure function values and the wind velocity and sonic temperature covariance statistics in the preflux data table (line 464).

The SlowSequence command is called to decrease the sampling frequency to 1 Hz for the remaining sensors and commands (line 471) that do not require high frequency sampling. Two important system diagnostics, the battery voltage and logger temperature, are sampled on lines 473 and 474. The voltage signal from the net radiometer and the two heat flux plates are sampled using the VoltDiff command (lines 475-477), and the soil thermocouple is sampled on line 478.

The commands for processing the raw turbulence data into corrected fluxes are also written within the SlowSequence structure. Due to the particulars of the SlowSequence command, the preliminary turbulent statistics, i.e., the wind velocity and sonic temperature covariance statistics and the structure function values, must be calculated before the other post-processing functions are executed. As a result, the preliminary turbulent statistics in the preflux data table, and hence the final eddy covariance and surface renewal fluxes from the logger program and the diagnostic variables associated with the velocity field, are based on the first 1799 seconds of data in the 30 minute (1800 second) interval.

The wind velocity, sonic temperature covariance statistics, and the structure function values are called into the program from the preflux table (line 488). The covariance statistics are used to calculate the two-dimensional coordinate rotation angles (lines 492-495). The rotation is applied to the vertical velocity and sonic temperature covariance to obtain the tilt-corrected vertical temperature flux (line 496), which is converted to H (line 497). The coordinate rotation is also applied to the wind velocity covariance statistics to obtain the

Variable	Definition	Units
Tpanel	Logger temperature	C
BattVolt	Mean battery voltage	V
Tc0	Mean air temperature measured by the thermocouple	C
St1	Mean soil temperature	C
u_bar	Mean horizontal wind speed	$m\ s^{-1}$
ustar	Friction velocity	$m\ s^{-1}$
tke	Turbulent kinetic energy normalized by mass	$m^{-2}\ s^{-2}$
tau	Momentum flux density	$N\ m^{-2}$
pitch	Sonic anemometer pitch angle	Degrees
azimuth	Wind direction angle	Degrees
Tsa	Sonic temperature ramp amplitude	K
TsDS	Sonic temperature ramp period	s
Tca	Air temperature ramp amplitude measured by thermocouple	C
TcDS	Air temperature ramp period measured by thermocouple	s
Rn	Net radiation	$W\ m^{-2}$
G	Ground heat flux density	$W\ m^{-2}$
TcH_SR	Surface renewal sensible heat flux density measured by the thermocouple	$W\ m^{-2}$
TsH_SR	Surface renewal sensible heat flux density measured by the sonic temperature	$W\ m^{-2}$
H_ECraw	Eddy covariance sensible heat flux density without tilt correction	$W\ m^{-2}$
H_ECrot	Eddy covariance sensible heat flux density with tilt correction	$W\ m^{-2}$
LE_ECraw	Latent heat flux density as the energy balance residual using *Rn*, *G*, and *H_ECraw*	$W\ m^{-2}$
LE_ECrot	Latent heat flux density as the energy balance residual using *Rn*, *G*, and *H_ECrot*	$W\ m^{-2}$

Tab. 2 - Definition of variables in the final output table (i.e., data table EB) of the logger program.
Tab. 2 - Definizioni delle variabili nella tabella dei risultati (cioe' la data table EB) del programma per datalogger.

tilt-corrected momentum flux density (line 499). The mean horizontal wind speed, the turbulent kinetic energy, the wind pitch angle, and the wind azimuth angle are calculated (lines 500-510) for use as diagnostic variables in data quality control by the user.

Starting on line 516, the ramp amplitude and ramp period from the sonic temperature are resolved using the Van Atta (1977) procedure. The sign of any positive third- and fifth-order structure function values are changed to negative values to ensure that the analytical solution succeeds over a greater range of lags (line 517 and 518). The cubic polynomial coefficients, *p* (Equation 11b) and *q* (Equation 11c), are calculated from the structure function values (lines 519 and 520). Another term, *D*, is derived from *p* and *q* to determine whether the cubic polynomial has three real roots or only one real root (line 521). If *D* is less than or equal to zero, the cubic polynomial is solved trigonometrically (lines 522-533). If *D* is greater than zero, the cubic polynomial is solved algebraically (lines 534-544). After the computation, the sign of the ramp amplitude in the sonic temperature data is recovered, i.e., set to the opposite sign as the original third-order structure function, and the ramp period is calculated (line 547-553). The ramp characteristics are used to calculate the surface renewal *H* (line 555). The surface renewal *H* from the thermocouple is calculated in the same manner on lines 557-597.

The net radiometer voltage signal is converted into *Rn* using its calibration factor (line 600). The net radiometer voltage signal, *Rn*, the ground heat flux plate voltage signals, and the soil thermocouple temperature are stored in the preRnG data table (line 603). Unlike the Kipp and Zonen NR-Lite instrument, some net radiometers require a correction that is dependent on wind speed. Although the preRnG data table could have been called earlier in this particular program, it is called after the horizontal wind speed calculation to facilitate modifying the program for other net radiometers.

The change in soil temperature from the beginning to the end of the measurement interval is calculated on line (607), and it is used to calculate the energy stored in the soil layer above the ground heat flux plates (line 610). The heat flux plate voltage signal is converted to an energy flux density using the plate calibration coefficients (line 613 and 614). The mean of the two ground heat flux plates is added to the energy storage in the soil layer above the plates to obtain G (line 615). After Rn, H, and G are determined, λE is calculated as the residual of the energy balance (line 619). The energy balance terms and the diagnostic variables are output on the EB data table (line 621).

5. RESULTS AND DISCUSSION

5.1. Comparison of energy balance terms from the logger program, EdiRe, and R

The output of the logger program is compared to the output of other flux processing programs to ensure that it is functioning properly. EdiRe does not have functions for G and Rn calculations, so comparing EdiRe and the logger program for these terms was not possible. These functions were written in the R computer language, and there were no differences in the Rn and G terms calculated in R and the logger program (Fig. 1a - b).

The logger-calculated H was compared against EdiRe and R (Fig. 1c). There were no differences between the tilt-corrected eddy covariance H from the logger program and from the R program. The R program was modified to calculate H (and the other turbulent statistics) on same 1799 second interval as the logger program. The differences in the H calculations between the logger program and EdiRe that arose from the additional second of data in the averaging interval are imperceptible in the regression analysis plots (Fig. 1c) and rounded statistics (Tab. 3). While it is technically correct to include the entire 1800 second interval in the turbulent flux calculations, because the Rn and G terms are calculated on this interval, it is clear that the final second of data does not appreciably impact the results. The error stemming from such minor discrepancies in the data interval is readily outweighed by the other errors associated with measuring turbulent fluxes (e.g., Foken 2008), including errors associated with uncertainty in the appropriate data interval for capturing the largest turbulent eddy scales (Lee *et al.*, 2004).

The latent heat flux density was calculated as the residual of the energy balance. There were no differences between λE flux calculations by the logger

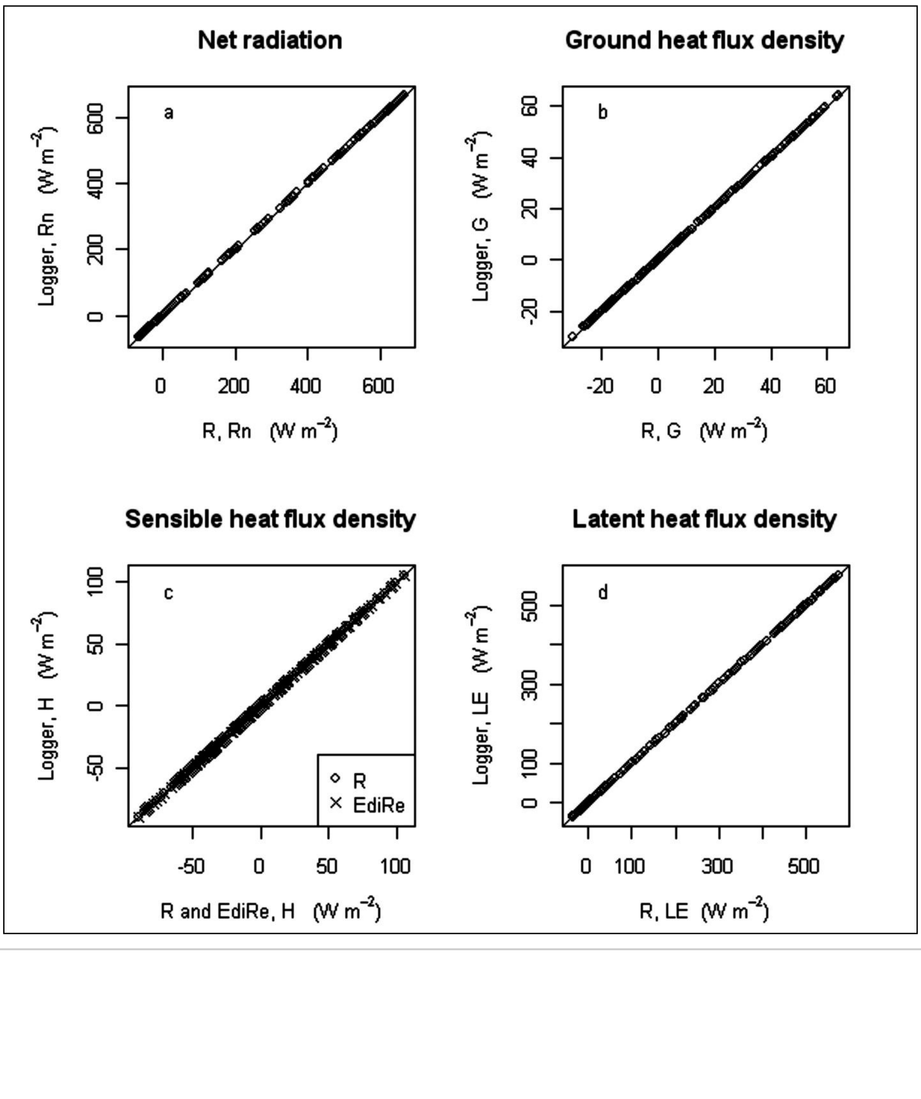

Fig. 1 - Linear regression plots for energy balance terms calculated by the logger program against energy balance terms calculated in R and EdiRe, including (a) net radiation, (b) ground heat flux density, (c) sensible heat flux density, and (d) latent heat flux density.

Fig. 1 - Regressioni lineari fra i componenti del bilancio energetico calcolati dal programma per datalogger e quelli calcolati con EdiRe e R: radiazione netta (a), flusso di calore nel suolo (b), flusso di calore sensibile (c) e flusso di calore latente (d).

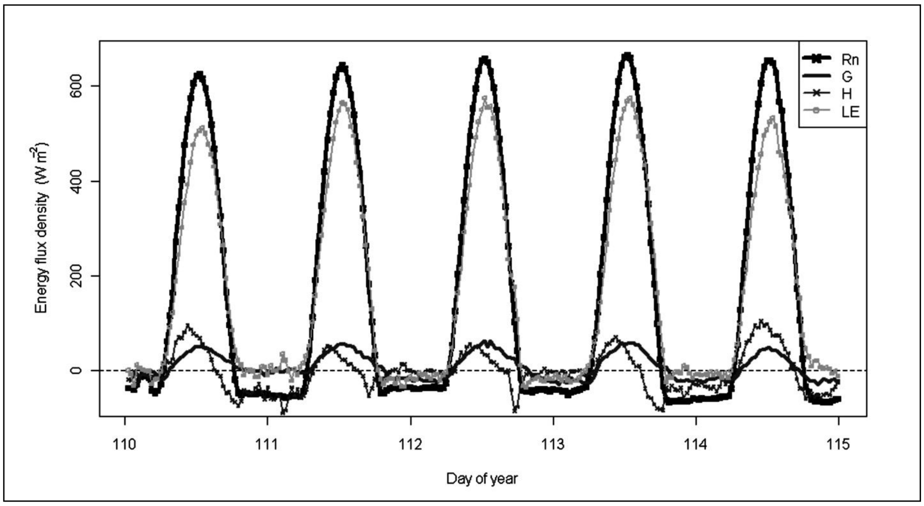

Fig. 2 - Diurnal energy balance flux densities.
Fig. 2 - Flussi giornalieri del bilancio energetico.

program and R (Fig. 1d). To make the comparison in the λE calculation between EdiRe and the logger program, the *Rn* and *G* terms were taken from the logger and *H* was taken from EdiRe because *Rn* and *G* were not calculated in EdiRe. The differences in λE between the logger program and EdiRe, arising from the differences in the data interval used in the *H* calculation, are negligible.

5.2. Interpretation of diurnal energy balance terms

Unlike laboratory experiments, ecosystem scale flux measurements are difficult to validate because experimental conditions cannot be controlled. An examination of the individual energy balance terms during fair weather conditions, such as those encountered in the present study, can provide some confirmation that the flux tower measurements and post-processing calculations are reasonable. The net radiation is positive during the day as the surface receives more radiation than it loses (Fig. 2), and negative at night as the surface loses more radiation than it receives, exhibiting the diurnal curve expected for sunny springtime days in a Mediterranean climate. The ground heat flux density also follows the expected diurnal curve (Fig. 2), and its greatest positive value is about 10% of the maximum *Rn*, which is reasonable for closed canopies (Allen *et al.*, 1998). It is positive during the daytime because energy is conducted from the surface into the ground, and negative at night as more energy is lost from the surface than received. The diurnal pattern in *G* is generally smooth, although there are small deviations likely resulting from sunflecks impinging on the ground directly over the ground heat flux plates. The ground heat flux density is measured at discrete spatial points, whereas the turbulent fluxes are indicative of broader areas, so errors stemming from the incongruity in the footprint of the turbulent fluxes and the available energy terms are expected in the energy balance measurements (Foken, 2008).

During the mornings, *H* was positive (Fig. 2), but in the afternoon it was negative. This is typical of actively transpiring crops in arid climates, where the crop canopy tends to be cooler than warmer air that moves over the surface in the afternoon due to regional advection. The additional sensible heat from regional advection contributes to water vaporization, so afternoon λE values were sometimes greater than the *Rn* values. During the evenings of day 110, 113, and 114, there was sufficient turbulent energy to drive

	R		EdiRe	
	m =	R^2 =	m =	R^2 =
Net radiation	1.00	1.00	--	--
Ground head flux density	1.00	1.00	--	--
Sensible heat flux density	1.00	1.00	1.00	1.00
Latent heat flux density	1.00	1.00	1.00	1.00

Tab. 3 - Linear regression coefficients through the origin for energy balance terms calculated by the logger program against energy balance terms calculated in R and EdiRe.
Tab. 3 - Coefficienti delle regressioni lineari forzate attraverso l'origine fra le componenti del bilancio energetico, calcolate dal programma datalogger e quelle calcolate con EdiRe e R.

negative sensible heat transfer. On the other hand, the evenings of day 111 and 112 showed H values near zero, suggesting that the eddy covariance technique could not resolve the flux or that little turbulent transfer was taking place.

The latent energy flux density follows the expected diurnal curve over a crop with adequate water during fair weather (Fig. 2). Net radiation is the dominant energy source for ET, so the λE values tracks the changes in Rn during the daytime. Over an actively transpiring crop, it is expected that the majority of the available energy during positive Rn conditions is partitioned into λE rather than H and G. During windy nights (i.e., days 110, 113, and 114), λE was near zero, whereas it was negative during calm nights, indicating condensation. While some condensation may have been occurring, there may also have been a slight bias in the estimation of the available energy terms (Rn and G), and therefore the negative λE values would be artifacts of the energy balance residual method. Nevertheless, the daytime contribution to λE greatly outweighs the nighttime contribution, so uncertainties in nighttime values are interesting but relatively unimportant.

5.3. Comparison of surface renewal and eddy covariance calculations of sensible heat flux density

The high coefficients of determination in the alpha calibration regressions for the surface renewal H measured with the sonic temperature and thermocouple and the sonic temperature (Fig. 3a and

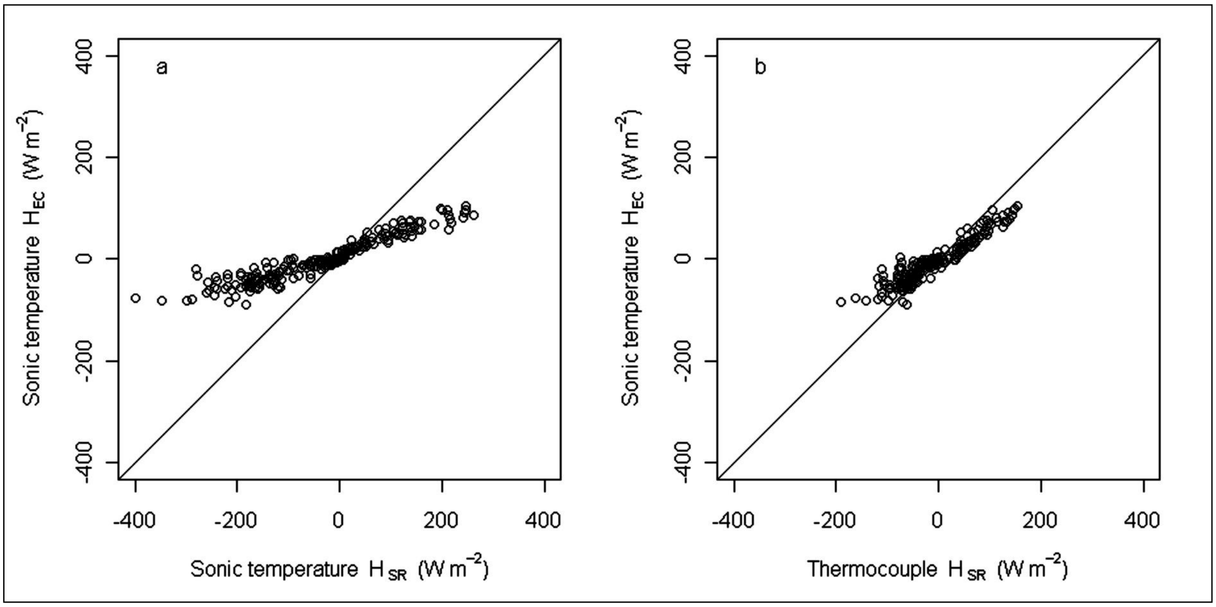

Fig. 3 - Plots of eddy covariance sensible heat flux density (H_{EC}) against surface renewal sensible heat flux density (H_{SR}) using the sonic and thermocouple temperatures. In (a) the sonic temperature is used for both the surface renewal and eddy covariance calculations, whereas in (b) the thermocouple temperature is used for the surface renewal calculation.

Fig. 3 - Regressioni fra il flusso di calore sensibile misurato con Eddy Covariance (EC) e quello misurato con Surface Renewal (SR) usando le temperature dell'anemometro sonico e delle termocoppie. In (a) la temperatura misurata dall'anemometro sonico è usata sia per i calcoli di EC che per i calcoli di SR. In (b) la temperatura delle termocoppie è usata per SR.

	Unstable		Stable		All	
	m =	R^2 =	m =	R^2 =	m =	R^2 =
Sonic temperature	0.42	0.93	0.24	0.88	0.29	0.84
Thermocouple	0.62	0.94	0.57	0.85	0.60	0.89

Tab. 4. - Linear regression coefficients through the origin for surface renewal sensible heat flux density against eddy covariance sensible heat flux density using either the sonic temperature or the thermocouple for the surface renewal calculation.

Tab. 4 - Coefficienti delle regressioni lineari forzate attraverso l'origine fra il flusso di calore sensibile calcolato con Eddy Covariance e calcolato con Surface Renewal, usando o la temperatura misurata dall'anemometro sonico o la temperatura misurata dalle termocoppie, per il calcolo con Surface Renewal.

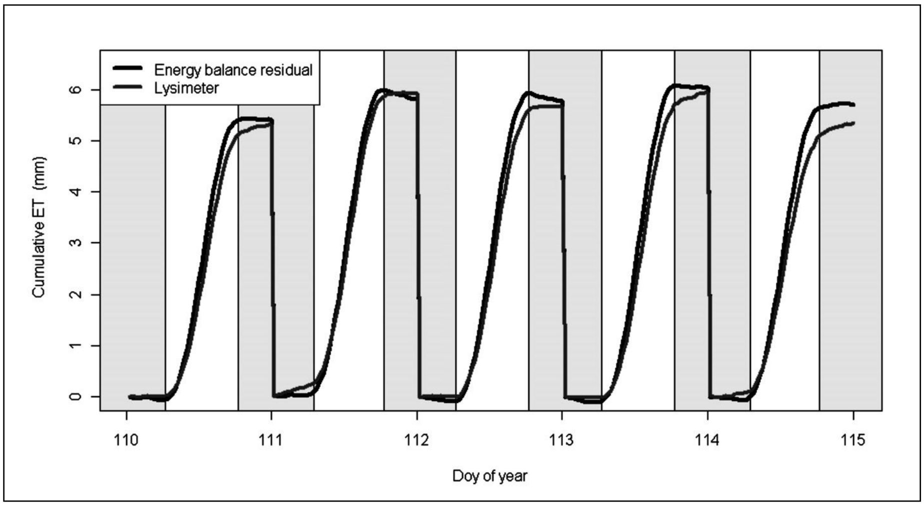

Fig. 4 - Cumulative daily evapotranspiration measured from the flux tower and from the lysimeter. Shaded background areas indicate negative net radiation values.
Fig. 4 - Evapotraspirazione cumulata giornaliera, acquisita mediante la torre di misura dei flussi e dal lisimetro. Aree a sfondo grigio indicano valori negativi di radiazione netta.

b, Tab. 4) are typical of the alpha calibration regressions from other studies (Paw U *et al.*, 1995; Snyder *et al.*, 1996; Spano *et al.*, 1997; Paw U *et al.*, 2005; Shapland *et al.*, 2012a), demonstrating that the logger program results are reasonable. The alpha calibration is lower when the sonic temperature is used for the scalar in the surface renewal calculation rather than the thermocouple signal for both unstable and stable conditions (Fig. 3a and b; Tab. 4). This occurs because the thermal inertia of the thermocouple attenuates the high frequency components of the time domain signal to a greater extent than the sampling volume spatial averaging of the sonic anemometer, leading to an underestimation of the scalar ramp characteristics (Shapland *et al.*, 2012b). As a result of this data artifact, the surface renewal *H* from the thermocouple signal aligns better with the eddy covariance *H* compared to the surface renewal *H* from the sonic temperature. Work is currently in preparation for the evaluation of a method for compensating the thermocouple signal for surface renewal measurements, and future versions of the logger program will include online thermocouple compensation (Shapland *et al.*, 2012b).

5.4. Comparison of cumulative daily evapotranspiration from the logger program and the lysimeter

The daily cumulative *ET* values from the logger program and the lysimeter agree well (Fig. 4). On most days, the cumulative *ET* from the logger program was slightly higher than the values from the lysimeter; however, the tower measurements represent fluxes from a broader and different area than the lysimeter measurements. Given that the wheat stand in the lysimeter was about 10 cm shorter and less dense than the plants in remainder of the field, higher *ET* values from the flux tower were expected. There are numerous other potential sources of error in *ET* measurements from flux towers (Lee *et al.*, 2000) and lysimeters (Pruitt and Angus, 1960), so the disparity between the measurement systems is not unreasonable.

6. CONCLUSIONS

The turnkey logger program was tested against independent software programs to demonstrate that the energy balance fluxes are correctly calculated. The diurnal energy balance curves from the flux tower and logger program follow the expected patterns for a crop field with adequate water in fair weather conditions, and the *ET* measurements from the flux tower agree well with the lysimeter measurements. The logger program renders micrometeorological methods more accessible for agricultural researchers and facilitates data processing and management. The output table containing the energy balance terms and the diagnostics variables can be downloaded using a remote or direct connection, adding significant convenience for program users during site visits.
The software presented here represents a core program that users can easily modify for other sensor configurations. The program and supplementary material can be downloaded at sites.google.com/site/tmshapland. We anticipate future releases of updated versions of the program as this is an ongoing project in our research efforts.

7. ACKNOWLEDGEMENTS

Partial support for this research was provided by J. Lohr Vineyards & Wines, the National Grape and Wine Institute, a NIFA Specialty Crops Research Initiative grant to AJM, and USDA-ARS CRIS funding (Research Project #5306-21220-004-00). The authors thank Diganta Adhikari, Frank Anderson, Cayle Little, Honza Rejmanek, Alfonso Russo, Mike Mata, and Gwen Tindula for their contributions and assistance in field testing the program.

8. REFERENCES

Allen R.G., Pereira L.S., Raes D., Smith M., 1998. Crop evapotranspiration: Guidelines for computing crop water requirements. FAO Irrigation and Drainage Paper 56. FAO, Rome, Italy.

DeVries D.A., 1963. Thermal properties of soils. *In:* Van Wijk, W.R. (ed.) Physics of the plant environment. North-Holland Publishing Co., New York, NY., U.S.A., 382 pp.

Doorenbos J., Pruitt W. O., 1977. Crop water requirements. FAO Irrigation and Drainage Paper 24. FAO, Rome, Italy.

DWR (Department of Water Resources), 2005. California Water Plan Update, Bulletin 160-05. California Department of Water Resources, Sacramento, CA., U.S.A.

Foken T., 2008. The energy balance closure problem. Ecological Applications, 18(6):1351-1367.

Jensen M.E., Burman R.D., Allen R.G., 1990. Evapotranspiration and irrigation water requirements. ASCE Manuals and Reports on Engineering Practice 70, American Society of Civil Engineers, New York, NY, U.S.A., 332 pp.

Mauder M., Foken T., Clement R., Elbers J. A., Eugster W., Grunwald T., Heusinkveld B., O. Kolle, 2008. Quality control of CarboEurope flux data – Part 2:Inter-comparison of eddy-covariance software. Biogeosciences, 5:451-462.

Lee X., Massman W.J., Law B.E., (eds.) 2004. Handbook of micrometeorology: A guide for surface flux measurement and analysis. Kluwer Academic Publishers, London, U.K., 250 pp.

Moratiel R., Martínez-Cob, A., 2011. Evapotranspiration of table grape trained to a gable trellis system under netting and black plastic mulching. Irrigation Science, 30(3):167-178.

Paw U K.T., Qiu J., Su H.B., Watanabe T., Brunet Y., 1995. Surface renewal analysis: a new method to obtain scalar fluxes without velocity data. Agricultural and Forest Meteorology, 74:119-137.

Paw U K.T., Snyder R.L., Spano D., Su H.B., 2005. Surface renewal estimates of scalar exchange. *In:*Hatfield, J.L. (ed.) Micrometeorology of agricultural systems. Agronomy Society of America, Madison, WI, U.S.A., 584 pp.

Pruitt W.O., Angus D.E., 1960. Large weighing lysimeter for measuring evapotranspiration. Transactions of the American Society of AgriculturalEngineers, 3(18):13-15.

R Development Core Team, 2012. R: A language and environment for statistical computing. R Foundation for Statistical Computing, Vienna, Austria.

Shapland T.M., McElrone A.J., Snyder R.L., Paw U, K.T., 2012a. Structure function analysis of two-scale scalar ramps. Part II: ramp characteristics and surface renewal flux estimation. Boundary-Layer Meteorology. 145:27-44.

Shapland T.M., Snyder R.L., Paw U K.T., and McElrone A.J., 2012b. Thermocouple frequency response compensation for surface renewal sensible heat flux measurements. (*In preparation*)

Shapland T.M., Snyder R.L., Smart D.R., Williams L.E., 2012c. Estimation of actual evapotranspiration in winegrape vineyards located on hillside terrain using surface renewal analysis. Irrig. Sci. 30(6): 471-484.

Snyder R.L., Spano D., Paw U K.T., 1996. Surface renewal analysis of sensible and latent heat flux density. Boundary-Layer Meteorology, 77:249-266.

Spano, D., Snyder, R.L., Duce, P., Paw U, K.T., 1997. Surface renewal analysis for sensible heat flux density using structure functions. Agricultural and Forest Meteorology, 86:259-271.

Synder R., Orang M., Geng S., Matyac S., Sarreshteh S., 2005. SIMETAW (Simulation of Evapotranspiration of Applied Water). California Water Plan Update 2005,Vol. 4: Reference guide, California Department of Water Resources, Sacramento, CA, U.S.A. Tanner, C.B., Thurtell, G.W., 1969. Anemoclinometer measurements of Reynolds stress and heat transport in the atmospheric surface layer. Research and Development Technical Report ECOM 66-G22-F to the US Army Electronic Command, Department of Soil Science, University of Wisconsin, Madison, WI, U.S.A.

Swinbank W.C., 1951. The measurement of vertical transfer of heat and water vapor by eddies in the lower atmosphere. Journal of Meteorology, 8(3):135-145.

Van Atta C.W., 1977. Effect of coherent structures on structure functions of temperature in the atmospheric boundary layer. Archives of Mechanics, 29:161-171.

Effect of Climate Variability and Climate Change on Crop Production in Tropical Wet-and Dry Climate

Abayomi Eruola[1], Niyi Bello[1], Gideon Ufeogbune[1], Akeem Makinde[2]*

Abstract: *Ibadan, Southwest Nigeria (Fig. 1A) is highly vulnerable to climate change due its geographic location in the tropical wet-and dry climate area and the strong dependence of its population on rain-fed agriculture. In the period 1981-2010, Ibadan experienced annual mean maximum temperatures ranging from 30.5°C to 32.5 °C, with an increase of around 0.5°C every ten years. The increasing mean maximum temperature in the last two decade after 1990's gave a consistent variation in rainfall, length of humid period, length of growing period and the onsets of rainfall with significant effect on the development, growth and final yield of the major food and cash crops in the study area leading to massive losses of agricultural production and shattered economies. Climate variability therefore poses one of the biggest obstacles to the achievement of food security and poverty reduction in the region.*
Keywords: *Ibadan, climate change, onset, growing season, humid periods.*

Riassunto: *L'Ibadan, Nigeria sud-ovest (Fig. 1A), è altamente vulnerabile al cambiamento climatico a causa della sua posizione geografica nella fascia climatica del tropico umido – secco, e della forte dipendenza della sua popolazione dall'agricoltura non irrigua. Nel periodo 1981-2010, l'Ibadan ha registrato una temperatura massima media annua tra i 30.5 e i 32.5 °C, con un incremento di circa 0.5 °C ogni 10 anni. L'aumento della temperatura massima media nelle ultime due decadi dopo il 1990 ha portato una consistente variazione del regime delle precipitazioni, della durata del periodo umido, della stagione di crescita e dell'inizio delle piogge, con un effetto significativo sullo sviluppo, sulla crescita e sulle rese delle principali colture alimentari e da reddito nell'area di studio, portando a massicce perdite di produzione agricola e ad crisi economiche. Pertanto la variabilità climatica rappresenta uno dei maggiori ostacoli al raggiungimento della sicurezza alimentare e alla riduzione della povertà nella regione.*
Parole chiave: *Ibadan, cambiamenti climatici, inizio stagione di crescita, periodi umidi.*

1. INTRODUCTION

Climate change through extreme temperature, frequent flooding and drought and increased salinity of water used for irrigation has become a recurrent subject of debate globally including Nigeria (Pachauri and Reisinger, 2007). Ibadan, capital of Oyo State, Southwest Nigeria is highly vulnerable to climate change due its geographic location in the tropical wet-and dry climate and the strong dependence of its population on rain-fed agriculture. Rainfall variability, land degradation and desertification are some of the factors that combine to make life extremely difficult in this part of the world. Like in most of Africa, agriculture is an important sector in this area given its multiple roles in food security, employment and contribution to national Gross Domestic Products (GDPs) ("Agbola and Ojeleye, 2007", "FAO, 2005"). The irrationality, however, is that agriculture in this area remains a highly under-developed sector, characterized by an almost total dependency on rainfall; low use of external inputs such as improved seeds and fertilizers; absence of mechanization; and poor linkage to markets. This makes agriculture highly vulnerable to climate change. Yet, people who depend on this activity for their livelihoods have faced a large variety of shocks (including climate variability and extremes) to which they have responded, based on traditional knowledge or by devising innovative measures when faced with new sets of constraints. Also, research over the last few decades has devoted a lot of efforts on the development of useful technologies in response to the various constraints and stresses facing agriculture in this region ("Showunmi and Akintola, 2010", "Ruddiman, 2003", "FAO, 2005"). The objective of this study is to assess and document the changes that have occurred in Ibadan, Southwest Nigeria over the last few decades and the consequences these changes have had on yield of some agricultural crops.

2. MATERIALS AND METHODS

2.1 Description of the Study Area

Ibadan (7° 54'N, 3°54'E) in Oyo State, Southwestern Nigeria covers an area extent of 3,080km² and is home to over 3.6 million people (Geo-Names geographical database). The area is characterized by a tropical climate with distinct wet and dry seasons with bimodal rainfall pattern and mean annual air temperature of about 30°C.

* Corresponding author e-mail: layosky@yahoo.com
[1] University of Agriculture, Abeokuta
[2] National Horticultural Research Institute, Ibadan
Received 16 September 2012, accepted 20 November 2012.

The annual rainfall totals ranges in the period between 850 and 1950mm. The major rock types found in the area are the Basement complex rocks of Precambrian age. A detailed analysis of this rock type by "Akintola, 1994" indicates that it can be further subdivided into the meta sedimentary series comprising mainly quartzites and migmatites complex comprising banded gneisses, augen gneisses and mig-matites (Fig. 1B). According to "Gbadegesin and Olabode, 1999", the soils of the Ibadan metropolis belong to the major soil group of ferruginous tropical soils and the soils of the Ibadan region can be further classified into four soil associations. All the four soil associations can be used for producing food crops such as cassava and maize but only one of these, the Egbeda soil association can be profitably used for producing tree crops such as cocoa and kola.

The inhabitant's livelihood strategies include agriculture, short and long-distance trading, and a variety of urban occupations. Traditionally, very little farming went on within the limits of Ibadan while the belt surrounding the town was used for cultivation of crops. The town land was used primarily for residential and public buildings, markets, shrine and paths (Fig. 1A). Only a small portion of the city land is used for production of vegetable. However, there are lots of pre-urban area within Ibadan were farming is largely the inhabitants occupation. Crops such as yam, sorghum, maize, cassava, cocoyam, Mellon, okra, tomato, pepper and vegetables are the major crops grown in the area. Farming in this region is almost entirely reliant on 6 to 7 months of rainfall.

2.2 Data collection and Analysis

Monthly meteorological data covering a period of 30 years (1981 - 2010) for Ibadan was used as required for this climate change study. The data used includes wind speed (m/s), mean temperature (°C), rainfall (mm), relative humidity (%), and sunshine hours (hours). Other required variables, with no measured values available were estimated using meteorological table (Shaw, 1994) for the estimation of potential evapotranspiration 'PE', have been used radiation received at the top of the atmosphere (Ra) in mm/day, daily maximum possible sunshine duration (N), mean saturated vapour pressure (ed), Blackbody radiation ($\sigma TK4$) in mm of water weighting factor for effect of temperature and altitude (W). Data on climate parameters for three decades (1981 – 2010) were collected from the Nigerian Meteorological Services, Ibadan (NIMET). The onset, length of growing season and humid periods were estimated using rainfall-potential evapotranspiration (P-PE) model according to the procedure of Cocheme and Franquin (1967). The Oyo state agricultural development programme, Ibadan, liaison office provided the corresponding crop yield data for the three decades. Data were also subjected to descriptive statistic to determine the relationship among temperature, water supply variable and crop yield. Also, table and graphs were used to enhance further illustration.

3. RESULTS AND DISCUSSION

Ibadan in the Tropical Wet-and Dry Climate, during the period 1981-2010 is characterized by strong climatic variations. Agriculture is predominantly rain-fed and depends on 6 to 7 months of rainfall with intermittent dry spells in between rains.

The study conducted in the last three decades in Ibadan showed annual mean maximum temperature ranging from 30.5°C to 32.5 °C, with the highest value of 32.3 °C in 1987, 1998 and 2004 and lowest value of 30.5 °C in 1993. In particular, low maximum temperature values less than 31.5 °C were monitored in 1981-1986 period; in 1987 an abrupt shift of approximately 1.5°C was observed. A range of temperature between 31.5-32 °C was observed between 1988-1992 and 1994-1998 with a very sharp fall experienced in 1993. A range of 31.2-31.7 °C between 1999-2003 and 2006-2009 was observed with increasing break of above 0.5 °C in 2004-2005. In general, an increase of about 0.5°C every ten years was observed as shown in Fig. 2.

This is in agreement with the now scientific consensus that the global climate is changing. Global mean temperature increased by 0.6 degree C in the last century, with the hottest years ever in record occurring after 1990. This warming of the world climate has been linked to a higher concentration of greenhouse gases (GHGs) in the atmosphere, the consequences of which can be manifested in the higher frequency of extremes such as floods, droughts and cyclones (Serigne *et al.*, 2006).

The tropical Wet-and-Dry climate in this study area has had its fair share of changes. The highest annual mean maximum temperatures experienced during 1987, 1994, 1998 and 2004 were accompanied by a sharp decline in rainfall.

The increasing mean maximum temperature in the last two decade after 1990's gave a consistent variation in rainfall, length of humid period, length of growing period and the onsets of rainfall. The range of annual rainfall for the considered period is between 850-1950 mm. In the two decades a drastic rise in rainfall between 1983 and 1985 has been monitored, followed by declining trend of rainfall up till the end of the 1980s (1991). The early 1990s is accompanied by irregular rise and fall of rainfall with sharp declining trend between 1996 and 1998 and a sharp rise in 1999. Furthermore, a relatively rise in rainfall pattern in the early 2000s between 2000 and 2005 and a stable rainfall for the remaining part of the decade.

This may be as a result of the also stable temperature monitored during this period.

The consistent variation in rainfall with varying degrees of severity that occurred especially in last two decades (1990s and 2000s) is likely going to have significant effect on the development, growth and final yield of the major food and cash crops in the study area. Climate variability therefore poses one of the biggest obstacles to the achievement of food security and poverty reduction in the region.

Observation from the study conducted in Ibadan (Fig. 3) showed a trend towards late onsets dates of rains over

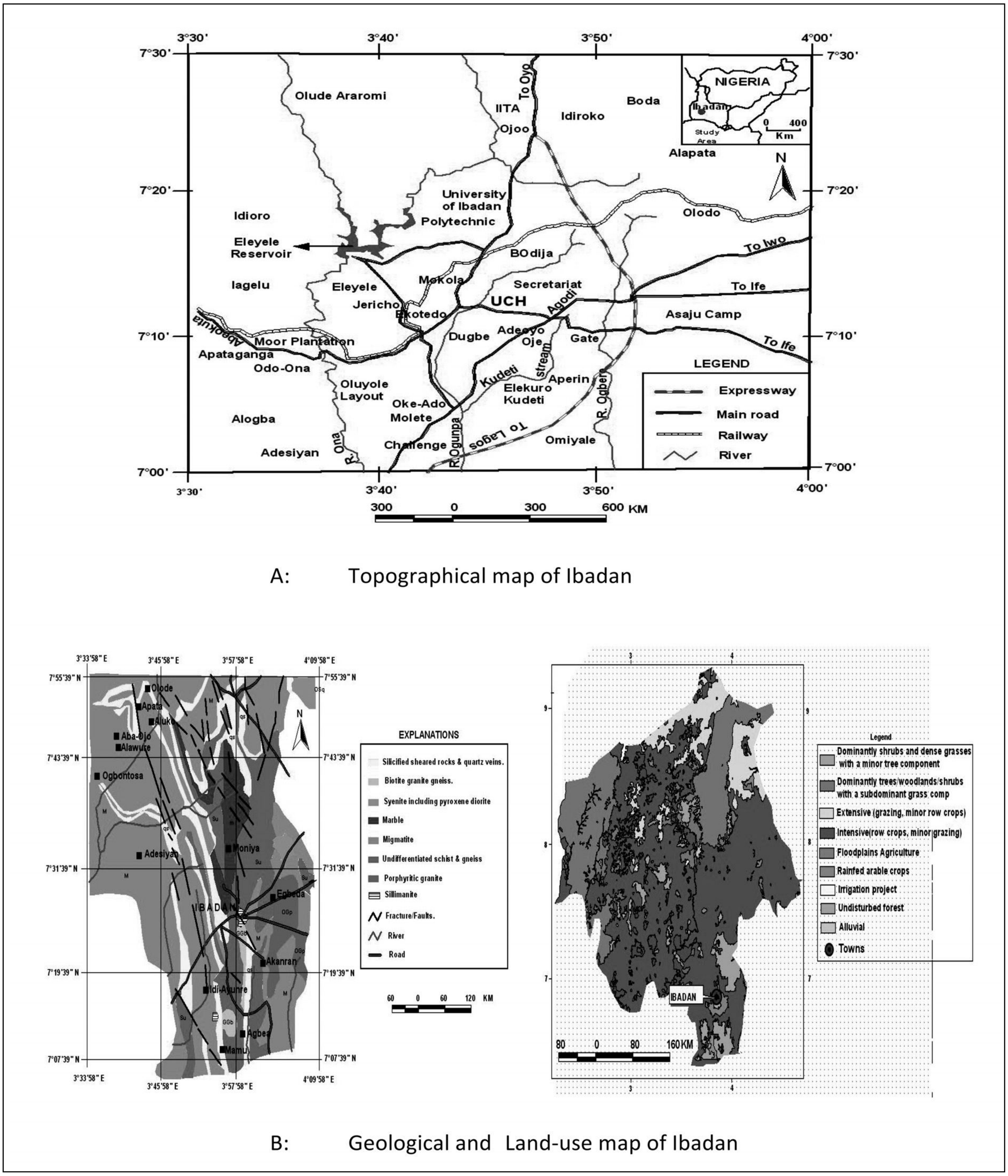

Fig. 1 - Map showing physical map of Ibadan in Oyo State, Southwestern Nigeria.
Fig. 1 - Mappa fisica della regione di Ibadan, Oyo State, Nigeria sud occidentale.

the last two decades of study (1990s and 2000s), with a abrupt decreasing shift occurring in 1991, 1996, 2003 and 2009. In these years, average onset date shifted from 100th day of the year (7th of April) to 45th day of the year (14th February) for early onsets and from average onset date 100th day of the year (7th of April) to 120th day of the year (27th April) for late onsets. The delayed onset has also been observed in recent years to cause shorter length growing seasons (Fig. 2). Similar studies conducted in Northern Benin (Houndenou and Hernandez, 1998) and in Cape Verde (see Cape Verde initial NC) also showed a decreasing trend in the duration of the wet season. The early onset of rains was observed to aid the yield of yam, cassava and pepper while the late reduced the yield. However, it was observed that there are no significant effect on tomato, maize and melon. This can be attributed to the low water requirement and length of growth of crops as compared to the past.
In the last two decades, Ibadan experienced two major dry spells years including 1983 and 1998, and the long period of sustained variation of rainfall that spanned the 1990s and most of the early 2000s. The annual average rainfall value of 1983 and 1998 were among the lowest ever recorded in the history of the Ibadan. In contrast, severe floods also occurred in 1985, 1996, 1999 and 2003 as illustrated by Fig. 4. Like in the onsets of rains, the rainfall variability also aids the yield of yam, cassava and pepper but had at the opposite contrary effect on tomato, maize and melon.
Observation from the study conducted in Ibadan (Fig. 5) also show a regular fluctuating trend of variation in length of growing season in the three decades of study, with the highest value of 280days in 2000s and lowest of 180 days in the 1990s. This fluctuating trend in length of growing season is as a result of variation in the onset of rains, cessation of rainfall, and rainfall distribution in the study area. It was observed that high fluctuating trend length of growing season aids the yield of yam, cassava and pepper while the low reduced the yield. However, it was observed that there are no significant effect on tomato, maize and melon. This can also be attributed to the low water requirement and length of growth of crops as compared to the past.

4. IMPLICATION OF CLIMATE VARIABILITY/CHANGE FOR THE STUDY AREA

4.1. The socio-economic impacts of the drying

The rainfall variability affected the study area with the tragic consequences on its people and economies as

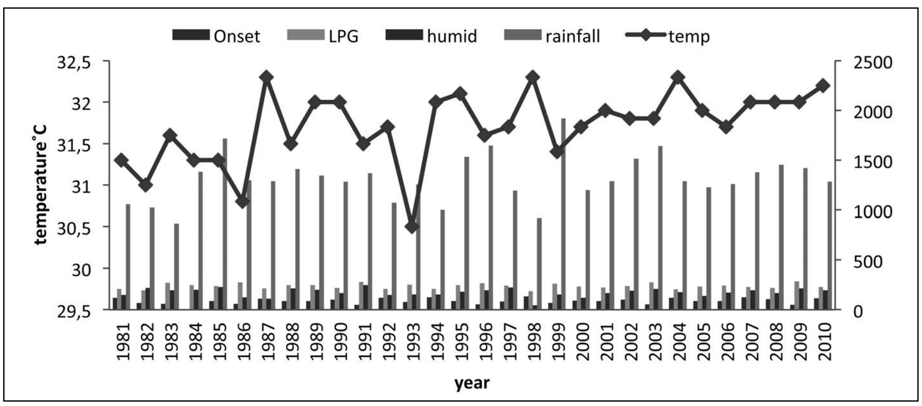

Fig. 2 - Graph showing average annual maximum temperature, onset, length of growing period (LGP), humid period and rainfall trend in the study area.
Fig. 2 - Grafico nella media annuale della temperatura massima, inizio e lunghezza (LGP) della stagione vegetativa, periodo umido e andamento delle precipitazioni nell'area studio.

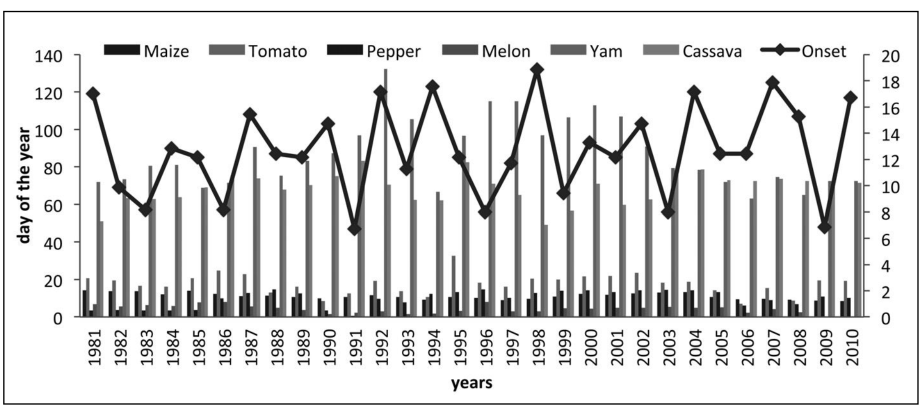

Fig. 3 - Graph showing onset of rain and yields of selected crops trend in the study area.
Fig. 3 - Grafico dell'inizio della stagione delle piogge e della produzione per le colture selezionate nell'area di studio.

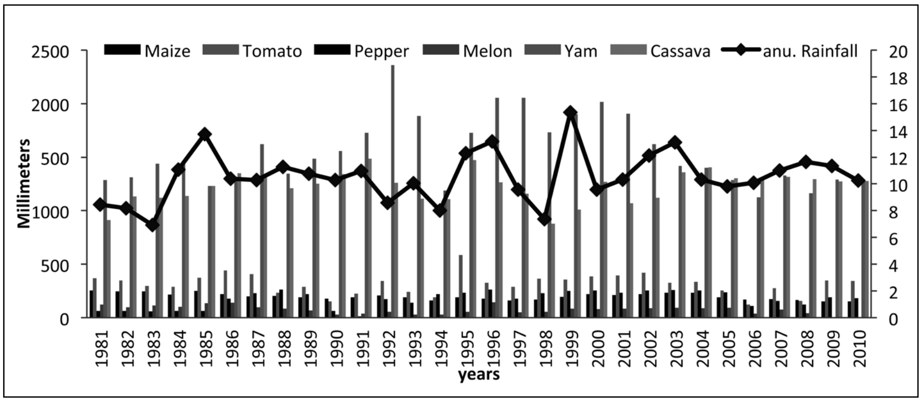

Fig. 4 - Graph showing annual rainfall and yields of selected crops trend in the study area.
Fig. 4 - Grafico delle precipitazioni e della produzione per le colture selezionate nell'area di studio.

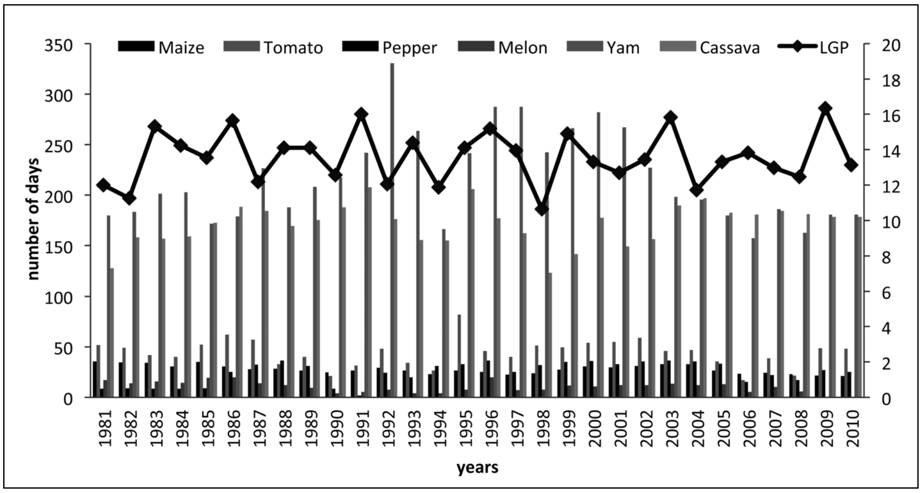

Fig. 5 - Graph showing Length of growing period (LGP) and yields of selected crops trend in the study area.
Fig. 5 - Grafico della lunghezza della stagione vegetativa (LGP) e della produzione per le colture selezionate nell'area di studio.

farmers find it extremely difficult to accurately determine the reliable beginning of the rain vis-à-vis start of the planting crops. Consequently, the schedules of farm operations are often wrongly phased and as a result incidence of failure of agricultural crops, replanting and ultimate low yield have characterized the agricultural food crops production in the study area with devastating consequences such as hunger and malnutrition as observed in the last 5 years in the last decade of the study in Ibadan and the deterioration of soil and water resources and desertification which has led to changing vegetation pattern of the area from rainforest to a derived savanna in the last decade. Many people migrated in search of relief to the neighbouring Lagos leading to squatter settlements and urban overcrowding increased, accompanied by rising unemployment.

4.2. Climate change and food security

Although there is no general consensus on the direction changes in precipitations will take in the future, climate change may have negative consequences on agricultural production and food security in the Nigeria and Ibadan in particular. If extremes in the form of dry spells and floods will be more frequent, additional pressure will be put on already stressed systems. This could induce a decline in crop production particularly yam, cassava and pepper causing a doubling of food prices. The combined effects of lower production on farming household and higher prices on the consumer's access to food raises the risk of hunger for the Nigerian population in nearby future.

5. CONCLUSION AND RECOMMENDATION

Rainfall variability is a major driver of vulnerability in Nigeria. However, blaming the 'environmental crisis' irregular annual rainfall alone would amount to a sheer oversimplification and misunderstanding of the tropical Wet-and-Dry climate dynamics. Climate is nothing but one element in a complex combination of processes that has made agriculture highly unproductive. The combined effects of population growth, land degradation (deforestation, continuous cropping and overgrazing), reduced and erratic rainfall, lack of coherent environmental policies and misplaced development priorities, have contributed to transform a large proportion of the tropical Wet-and-Dry climate area into derived savanna, resulting in the deterioration of the soil and water resources. The entangled processes of land degradation and desertification, which have prevailed in the tropical Wet-and-Dry climate over the last few decades, are nothing more than the embodiment of a degenerative process that started several decades back. The variation in the Onsets of rain, length of growing season, rainfall variability and dry spells in between rains were not necessarily the cause, but certainly the culmination, of this environmental crisis. Even if rainfall has come back to near-normal and food security improved in recent years, the tropical Wet-and-Dry climate remains an environmentally sensitive region and climate change is likely to exacerbate the vulnerability of its ecological and socio-economic systems.

5.1 Recommendations to make agriculture less vulnerable to climate change

1. Investment into agriculture by governments and international agencies in order to significantly address problems related to food insecurity and poverty in Africa.
2. Foster the use of climate and meteorological information to inform decision making: inter-annual variability of rainfall is a major constraint to agricultural sustainability in the study area. Since climate change will exacerbate this problem, using seasonal climate forecasts to inform farmers, herders and other users will be necessary to avoid surprises, allow good use of favorable conditions and make the right decisions in case of an impending drought.
3. Promote improved agricultural technologies\and the use of drought-tolerant and drought escaping crops/varieties in areas where water deficits will be more pronounced due low rainfall or high evapotranspiration.
4. Invest in soil and water conservation management strategies for sustainable crop production and buffering against drought and floods, which are likely to be more frequent with climate change.
5. Develop small scale irrigation schemes.
6. Invest in pest and disease control.
7. Develop low cost post-harvest technologies to prevent damage of grain stocks by insect and other storage pests.
8. Develop processing industries.
9. Provide modernize the livestock sub-sector.
10. Foster institutional linkages for agricultural sustainability through diffusion of technologies to reduce vulnerability.
11. Develop special rural micro-credit schemes for small-scale farmers.
12. Improve information delivery to enhance the adaptive capacities of the rural areas to climate change. Information on weather or new technologies can be transmitted to the farmers using rural radios and other media.
13. Invest in rural infrastructure.
14. Improve links to local, national and regional markets.

6. REFERENCES

Agbola T., Ojeleye D., 2007. Climate Change and Food Production in Ibadan, Nigeria.

African Crop Science Conference Proceedings. 8: 1423-1433.

Ajose S. 2010. "The Evolution and Development of Lagos State Administration in Lagos State: A Sociological Approach." http://www.cefolassaocoed.net/index.php

Akintola F., 1994. Geology and hydrology of the Ibadan region. Rex Charles Pub., Nigeria. 18-27 pp.

Cocheme J., Franquin P., 1967. An agroclimatological survey of a semi arid area in Sourth of the Sahara. WMO Technical note No. 86, Geneva.

FAO., 2005. Food security and the Escape from hunger cited 11th October 2005.

http.www.fao.org/docrep/w7442E/w7442e04.htm.

Gbadegesin A., Olabode M., 1999. The Soils of the Ibadan Metropolis: Nature and Characteristics. Land Contamination & Reclamation. 7 (3): 209-217.

Houndenou C., Hernandez K., 1998. Modification de la saison pluvieuse dans l'Atakora (1961-1990). Unexemple de sècheresse au nord-ouest du Bénin. Sécheresse 9: 23-34

Pachauri R., Reisinger A., ed., Climate Change 2007: Synthesis Report, Contribution of Working Groups I, II and III to the Fourth Assessment Report of the Intergovernmental Panel on Climate Change.

Ruddiman W., 2003. The anthropogenic greenhouse era began thousands of years ago. Climate Change 61 (3): 261-293.

Shaw M., 1994. Hydrology in practice. Van Nostrand Reinhold. Berkshire, UK. 245 pp.

Showunmi F., Akintola J., 2010. Effect of Climate variability on maize production in Nigeria. Research journal of Environmental and Health sciences.2 (1): 19-30.

Serigne T., Louis V., Jens M., 2006. Climate Change and Variability in the Sahel Region: Impacts and Adaptation Strategies in the Agricultural Sector.

UN-HABITAT. 2006. *Lagos: Bridging the Urban Divide*. Nairobi.

Runoff in Cultivated Hilly Areas as Influenced by Crops and Land Management

Linda Pieri[1], Francesca Ventura[1], Nicola Gaspari[1], Fiorenzo Salvatorelli[1], Giuliano Vitali[1], Paola Rossi Pisa*

Abstract: *Runoff is one of the major causes of soil loss in the hilly areas of Italy. It is possible to successfully prevent the phenomenon by an adequate drainage of water in the agricultural areas, via the modeling of soil surface, and choosing the proper tillage and crop. The best soil management is selected by a deep knowledge of the chemical and physical properties of soil, of the topography and the land use. In order to study the problem in detail, a field experiment was carried out in the hillside next to Bologna, Italy (Ozzano dell'Emilia, 44°24'N, 11°28' E, 185 m a.s.l.) for a 17-year-long period (1992-2009). In this experiment the effect on runoff of field crops (maize, wheat, sorghum, alfalfa and rye-grass) and orchard (cherry trees), with different slopes and land modelling, was evaluated. The crops were cultivated with various field modeling, in 5 plots of 1000 m² each (50m x 20m). The soil was sandy-loam and the tillage management was performed as in the common practice of the area. Precipitation was continuously measured by a meteorological station next to the plots and each plot was equipped with runoff ditches and measurement gauges. Results show that, between the multiannual crops, cherry trees orchard was always more efficient than alfalfa in minimizing runoff, and independently from slope. As an average of the entire period, the number of runoff events was the highest in the plots diagonally cultivated and was the lowest in the plot cultivated following the contour lines. The up-and-down modelling gave good results in controlling the runoff. A significant relationship was evidenced between the total amount of rainfall during the crop year (from October to September) and the mean number of runoff events, irrespectively of the crop.*
Keywords: *land management, land modeling, long term experiment, runoff, slope, slope length.*

Riassunto: *Il runoff costituisce una delle principali cause di perdita di suolo nelle zone collinari italiane. Attraverso un'adeguata gestione del suolo, basata su appropriate scelte di sistemazione idraulica delle aree coltivate, di coperture vegetali e di operazioni agronomiche, è possibile limitarne le conseguenze. Allo scopo di studiare l'argomento in dettaglio, è stato allestito un esperimento di campo di lunga durata, 17 anni (1992-2009), in una zona collinare della provincia di Bologna (Ozzano dell'Emilia, 44°24'N, 11°28' E, 185 m s.l.m.), dove sono stati valutati gli effetti sul ruscellamento di diverse coperture vegetali, sia erbacee (mais, frumento, sorgo, erba medica, loietto), sia arboree (ciliegio da legno), pendenze (da 0.65% a 17%) e sistemazioni dei terreni (giropoggio, ritocchino, diagonale). Lo schema sperimentale era costituito da 5 parcelle di 1000 m² (50mx20m), ciascuna caratterizzata da una diversa pendenza e sistemazione. La granulometria delle zona sperimentale è sabbioso-medio impasto e la gestione agronomica ha seguito le comuni pratiche agricole della zona. La precipitazione è stata misurata in continuo, grazie ad una stazione meteorologica situata accanto alle parcelle; ciascuna parcella è stata circondata da scoline, per garantirne l'isolamento idrologico, ed equipaggiata con strumenti di misura e campionamento del ruscellamento. I risultati hanno mostrato che tra le colture pluriennali la parcella occupata dai ciliegi da legno ha sempre prodotto una minore quantità di runoff rispetto all'erba medica, indipendentemente dalla pendenza. Come media dell'intero periodo, il numero degli eventi di runoff è stato più alto nelle parcelle lavorate diagonalmente, mentre la parcella che ha fornito i minori quantitativi di runoff è stata quella a giropoggio. Anche la parcella lavorata a rittochino ha manifestato una buona capacità di controllare il ruscellamento. Infine, una significativa relazione è stata messa in evidenza tra la quantità di pioggia durante l'annata agraria (da ottobre a settembre) e la media del numero di eventi di ruscellamento, indipendentemente dalla copertura vegetale.*
Parole chiave: *gestione del suolo, sistemazioni colturali, esperimento di lunga durata, runoff, pendenza.*

INTRODUCTION

Runoff is the fraction of rainfall reaching the soil surface which doesn't infiltrate nor penetrate into the soil by preferential flow in cracks, feeding directly the surface hydrological network. Runoff is considered one of the major erosion factors and sediment carrier agent. It also represents a principal reason for soil degradation and loss of fertility, reducing water storage capacity, with negative effects on agricultural management practices and effectiveness. Beyond that, runoff water carries with it dissolved chemicals and soil particles determining erosion and water pollution. From the view-point of surface hydrology, runoff is characterized by an irregular flow regime, strictly dependent from that of precipitations, and represents the phenomenon behind river overflows and plain flooding (Luino, 2005).

As runoff is mainly driven by rainfall, it is fundamental

* Corresponding author: e-mail: francesca.ventura@unibo.it
[1] DipSA-Agricoltural Department, University of Bologna, Italy
Received 19 July 2012, accepted 20 October 2012.

to parameterize the precipitation in terms of amount, intensity and erosivity. In literature a number of relations between rainfall intensity and the amount of soil loss from runoff have already been proved (Romkens *et al.*, 2001).

Both in the case of runoff and erosion, a fundamental role is given by vegetation canopy, surface slope and, in agriculture, soil management, such as field modeling type and direction (Ampofo *et al.*, 2002; Zhang and Garbrecht, 2002, Takken *et al.*, 2001a, Takken *et al.*, 2001b, Souchere *et al.*, 1998). Several studies show that a vegetation cover can strongly reduce runoff (Baumhardt and Jones, 2002; Fisher *et al.*, 2002; Rossi Pisa *et al.*, 1999; Rossi Pisa *et al.*, 1996), decreasing droplets impact energy at the soil surface, related to soil disaggregation and particles detachment (Wischmeier and Smith, 1978). In general, natural forests are subject to neglectable erosion because of their multilayered canopy given by trees, underwood and litterfall that protects surface from rain droplets impact enhancing infiltration (Grace, 2002). On tilled fields the choice of species and of cropping techniques strongly determine surface roughness and drives the origin of rills and gullies (Leys *et al.*, 2010, Takken *et al.*, 2001, Souchère *et al.*, 1998, Ludwing *et al.*, 1995, Desmet and Govers, 1997).

Aim of this investigation is the evaluation of relationships between runoff, overall in terms of number and amount of events, vegetation cover, agronomical practices and land modeling, and soil slope, by means of a long-term experiment (17 years) performed on cropped plots with a uniform slope.

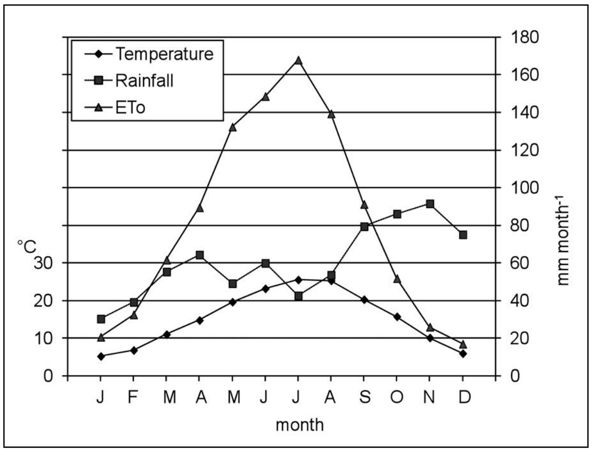

Fig. 1 - Bagnouls & Gaussen climatic characterization of the experimental site of Ozzano dell'Emilia (BO) Italy – 185 m a.s.l, in the period 1992-2009. Temperature is in °C, rainfall and evapotranspiration in mm/month.

Fig. 1 - Caratterizzazione climatica di Bagnouls & Gaussen del sito sperimentale di Ozzano dell'Emilia (BO), Italia - 185 m s.l.m. nel periodo 1992-2009. La temperatura è in °C, la pioggia e l'evapotraspirazione in mm/mese.

MATERIALS AND METHODS

The experiment has been carried out in the farm of the University of Bologna, located in the hilly area of Ozzano dell'Emilia, (44°24'N, 11°28' E, 185m a.s.l.). The soil is a sandy loam, classified as Typic Ustochrept (Rossi *et al.*, 2000).

An automated agrometeorological station is installed in the experimental area, the climate of the area is represented in Fig. 1, by means of a Bagnouls and Gaussen graph. The period of aridity goes from mid

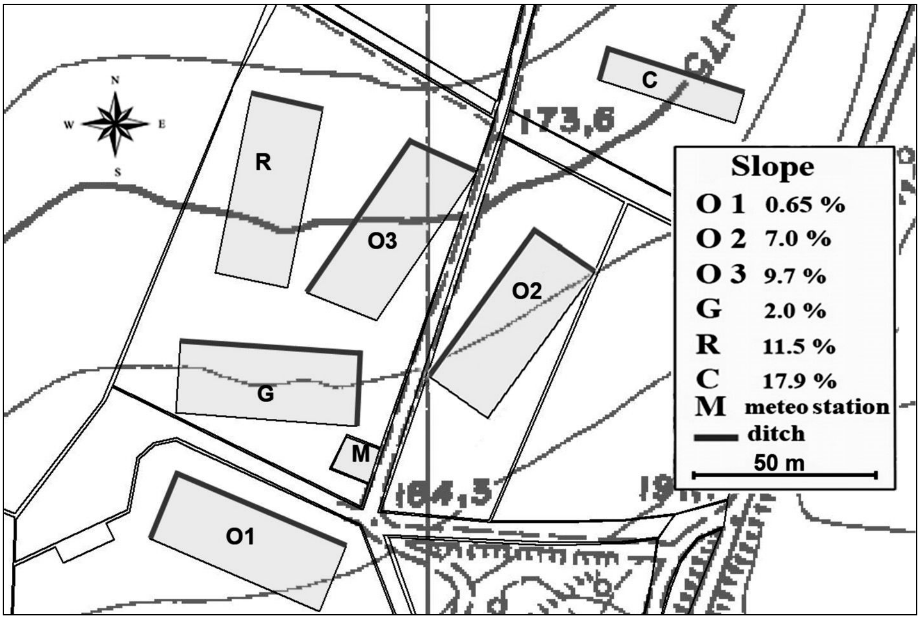

Fig. 2 - Map of the experimental area. Plots, ditches, and the contour lines are in evidence.

Fig. 2 - Mappa dell'area sperimentale. Sono evidenziate le parcelle, le scoline e le linee di livello.

Plot	Tillage direction	Slope (%)
O1	diagonal	0.65
G	contour line	2.0
O2	diagonal	7.0
O3	diagonal	9.7
R	up-and-down	11.5
C	up-and-down	17.0

Tab. 1 - Tillage direction and slope of the plots.
Tab. 1 - Sistemazione e pendenza delle parcelle.

June to the beginning of September. In the period of trial (1992-2009), the mean air temperature was 15°C, about 1°C higher than the previous 20 years, while the average annual precipitation was 717 mm. Together with the rainfall amounts the intensity was measured, in mm/10'.

The experiment was held on five rectangular hydraulically isolated plots (Fig. 2), each of 1000 m^2, with sides of 50 m and 20 m, with the slopes and hydraulic-agricultural management as shown in Tab. 1 (Rossi Pisa *et al.*, 1986). Open ditches were dig on the perimeter of each plot, parallel to the sides of the rectangular plots, the runoff water was collected only from the ditches that are thick in Fig. 2, and then transported to the measurement device. The runoff mean path in each plot depends on the slope and tillage

Crop-year	Crop	Sowing	Harvesting	Tillage					
				type	date	type	date	type	date
1992 – 1993	Maize	4/19/1993	09/06/1993	Harrowing 10cm	2/17/1993	Residues mulching	09/10/1993		
1993 – 1994	Wheat	10/29/1993	07/11/1994	Harrowing 10cm	09/17/1993	Harrowing 10cm	10/15/1993		
1994 – 1995	Sorgum	05/03/1995	09/07/1995	Harrowing 10cm	04/28/1995	Residues mulching	09/12/1995		
1995 – 1996	Wheat	10/13/1995	07/05/1996	Plowing 25cm	09/18/1995	Harrowing 10cm	10/03/1995	Plowing 50cm	08/15/1996
1996 – 1997	Sorgum	05/02/1997	09/05/1997	Harrowing 10cm	04/08/1997	Mulching	09/11/1997		
1997 – 1998	Wheat	10/17/1997	07/06/1998	Plowing 35cm	09/11/1997	Harrowing 10cm	10/17/1997	Residues mulching	07/30/1998
1998 – 1999	Sorgum	05/03/1999	09/06/1999	Plowing 35cm	08/01/1998	Harrowing 10cm	10/26/1998	Residues mulching	09/20/1999
1999 – 2000	Wheat	11/02/1999	06/22/2000	Plowing 35cm	09/23/1999	Harrowing 10cm	09/29/1999	Plowing 45cm	07/24/2000
2000 - 2001	Alfalfa	3/22/2001	02/05/2001, 06/26/2001	Harrowing 10cm	09/29/2000	Harrowing 10cm	06/11/2000		
2001 - 2002	Alfalfa		05/22/2002, 06/18/2002, 07/23/2002, 09/03/2002	tedder 3-4 times per year					
2002 - 2003	Alfalfa		05/20/2003, 06/30/2003						
2003 - 2004	Alfalfa		05/19/2004, 06/28/2004,						
2004 - 2005	Alfalfa		05/20/2005, 06/23/2005, 07/25/2005, 09/05/2005						
2005 - 2006	Alfalfa		05/11/2006, 06/20/2005, 07/18/2006, 08/28/2006						
2006 - 2007	Alfalfa		04/24/2007, 26/11/2007, 07/10/2007, 08/27/2007						
2007 - 2008	Rye-grass	10/02/2007	06/05/2008, 06/17/2008, 08/18/2008	Disking 10cm	09/03/2007	Harrowing 10cm	09/12/2007		
2008 - 2009	Rye-grass		05/19/2009						

** Recording of runoff data on the rye-grass plot was stopped at the end of 2009.*

* La registrazione dei dati di ruscellamento della parcella di loietto è stata interrotta alla fine del 2009

Tab. 2 - Crop rotation in the plots O1, O2, O3, G and R, date of sowing, harvesting and of the main tillages. All plots were treated in the same way in the same year, all the tillages were performed using open field equipments.
Tab. 2 - Successione colturale nelle parcelle O1, O2, O3, G e R, data di semina e delle principali operazioni agronomiche. Tutte le parcelle sono state sottoposte alla stessa gestione agronomica, utilizzando macchine da pieno campo.

direction, going from a minimum path of 20 m for G, to a maximum of 50 m for R. All the agricultural managements (tillage, sowing, fertilization, agrochemical treatments, harvesting, etc.) were performed following the direction of the longest side and using the common machineries of the farm. The details of the management are reported in Tab. 2.

The study period ranges from 1992/93 to 2008/09, considering the crop year (from October to September). All plots were cultivated with the rotation typical of the region, based on macro thermal herbaceous crops, namely sorghum and maize, and micro thermal, the winter wheat. From 2001 to 2007 all plots were cultivated with alfalfa and from 2007 to 2009 with rye-grass (Tab. 2).

In 1996 one more down-hill plot of 360 m^2 (9 m x 40 m) and 17% of slope was added, selecting an appropriate area into a 10-year-old cherry orchard (*Prunus avium* L.).

Runoff was collected by open ditches, settled downhill (Fig. 2) and carried by aluminum pipes to steel containers (internal size 70x70x70 cm^3). The containers have a triangular spillway at 50 cm from the bottom; from here the water and sediment fell into a tipping bucket (Fig. 3) which records, by means of a data logger, the amount of water overflowed from the container. This device is used only in case of intense runoff events, most of the times the container capability is enough.

The number of events and overflows occurred in each plot was recorded all along the study period, while in the sub-period 1996 to 2002 the amount of runoff water collected from all the plots (except for the plot R) was also recorded.

Fig. 3 - Experimental station for the measurement of runoff and the collection of samples.

Fig. 3 - Stazione sperimentale per la misura di runoff e la raccolta dei campioni.

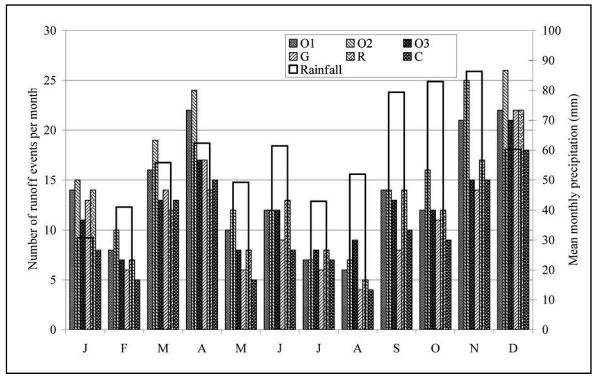

Fig. 4 - Distribution of the number of runoff events per month, for the six plots. The empty columns show the mean monthly precipitation.

Fig. 4 - Distribuzione del numero degli eventi di ruscellamento per le sei parcelle. Le colonne vuote mostrano la precipitazione media mensile.

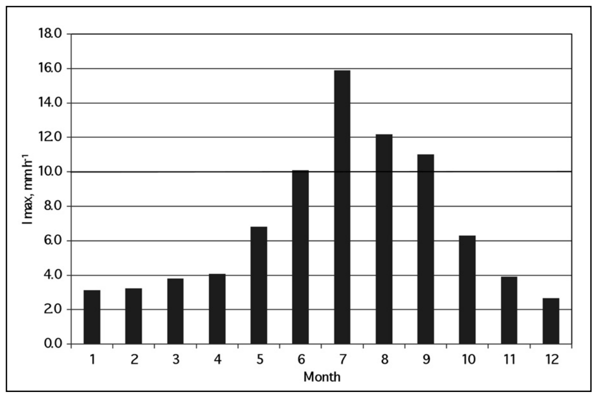

Fig. 5 - Monthly average of the recorded maximum intensity of rainfall, in the period 1992-2009. Notice that Imax = 10 mm h^{-1} is defined by the UK Met Office as "heavy rain".

Fig. 5 - Media mensile dell'intensità di pioggia massima registrata nel periodo 1992-2009. Da notare che Imax = 10 mm h^{-1} è definita "pioggia forte" dall' UK Met Office.

RESULTS AND DISCUSSION

3.1 Relationship between rainfall and runoff events

Precipitation pattern during the years 1992 – 2009 shows a monthly distribution characterized by two picks, in Spring (secondary) and Autumn (principal), as in Fig. 1. This characteristic remains when dealing only with the rainfall that produced runoff. In particular, in this case, the secondary pick was in April and the principal in November/December, as shown by monthly precipitation in Fig. 4. In this figure, it is also evident that the maximum number of runoff events occurred in these two periods. Fig. 5 shows Imax in mm per hour, average of the considered

Date	Rainfall			Runoff			
	mm	Int max (mm/h)	EI(30)	Hmax (mm)		Hmin (mm)	
05 Sep, 1996	32.4	70.8	172.8	0.33	O3	0	G
19 Sep, 1996	53.8	39.6	164.5	0.21	O2	0	G
07 Oct, 1996	177.2	21.6	244.6	143.41	O2	58.47	O1
14 Oct, 1996	18.0	15.6	25.6	0.47	O2	0	G
14 Sep, 1997	34.0	21.6	62.5	0.28	O1	0	O3,G
04 Sep, 1999	47.0	48.0	303.2	0.06	O1	0	O3,G
11 Oct, 2000	14.4	7.2	6.3	0.12	O1	0	O2,O3,G
21 Oct, 2001	27.4	44.4	112.7	0.03	G	0.01	O1
15 Jul, 2002	44.6	43.2	89.6	0.04	G	0.01	O1
18 Jul, 2002	30.6	62.4	185.8	0.07	O1	0.02	O3,G
24 Jul, 2002	11.2	9.6	8.2	0.11	O1	0	G
07 Aug, 2002	10.4	14.4	8.5	0.01	G	0	O1,O2,O3
10 Aug, 2002	21.6	7.2	17.7	0.02	G	0	O1
23 Aug, 2002	29.0	82.8	271.3	0.04	O3	0.02	O2
26 Aug, 2002	12.0	20.4	21.8	0.01	G	0	O1
28 Aug, 2002	17.6	52.8	107.4	0.03	G	0	O1,O2,O3

Tab. 3 - Detailed description of the late summer-early autumn runoff events in the sub-period 1996-2002. For each event the quantity, intensity and 30-min rainfall erosivity index EI_{30} were calculated. The runoff is characterised by the maximum and minimum recorded amount, and the plots where they occurred.
Tab. 3 - Descrizione dettagliata degli eventi di runoff avvenuti alla fine dell'estate o all'inizio dell'autunno nel sotto-periodo 1996-2002. Per ogni evento sono stati calcolati: quantità, intensità, indice di erosività EI_{30} *della pioggia. Per il runoff sono state indicate: la quantità massima e minima registrata e le parcelle dove queste quantità sono state registrate.*

period. Notice that the summer months have Imax > 10 mm h^{-1}, limit that define the "heavy rain" by the UK Met Office, and the pick is in July. The actual maximum, during the considered period, was of 22 mm/10', for a total amount of 177.2 mm in the event, recorded on the 10th of July, 2006. This very heavy rainfall occurred on the bare soil after the harvesting of wheat and the main plowing (50 cm deep), producing a runoff of 143.4 mm in O2 (Tab. 3).
As reported by Fang (2012), rainfall characteristics are decisive for the relative importance of different storms in the runoff generation mechanisms, while Nadal-Romero *et al.* (2008) suggested that local storm patterns is fundamental in determining the shape of the runoff hydrograph. In this research, a linear relationship between the rainfall amount during the crop year and the average number of runoff events was found, when considering results from plots with herbaceous crops, regardless of species and plot slope (modeling) (Fig. 6). This confirms the rainfall main role in runoff formation, since the other factors, i.e. the physical characteristics of soil, are the same.
During the sub-period 1996-2002, forty-six rainfall events produced runoff, at least in one plot. The most erosive events occurred during summer/autumn, and are detailed in Tab 3. The table shows the rainfall amount, the maximum intensity, and the 30 minutes erosivity index of rainfall, as used in the Universal Soil Loss Equation for predicting soil loss from agricultural hill slopes (Wischmeier, and Smith, 1978) only for the end-of-summer/early-fall events. In the second half of the table the maximum and minimum height of runoff are shown, together with the plot/plots where they

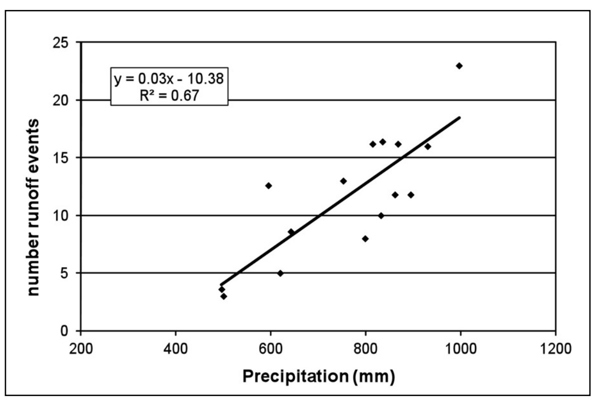

Fig. 6 - Runoff events number (mean of the plots) as a function of the annual precipitation in the period 1992-2009.
Fig. 6 - Numero di eventi di runoff (media delle parcelle) in funzione della precipitazione annuale nel periodo 1992-2009.

occurred. Generally in this period the precipitation find dry soils, crops already harvested or at the end of the cycle, with low evapotranspiration and poor ground coverage. All these factors, together with the high intensities of rain, makes late summer/early autumn the most dangerous period for erosion.
ANOVA statistical analyses show correlations between the runoff amount and the rainfall characteristics for each plot, varying the soil vegetation cover. When the vegetation covers completely the ground, there is a significant correlation between rainfall amount and runoff for O3 and G ($p<0.05$). Moreover, during low crop cover stages (about 50% of coverage), we found significant correlation in O1 ($p<0.05$). In general the vegetation cover effect is not always directly correlated with runoff, due to the complexity of the process (Ventura *et al.*, 2004; Pieri *et al.*, 2009).

3.2 Crop effect on runoff

The proportion of soil surface that is bare and therefore exposed to raindrop impact and crusting follows land use. This factor influences interception and surface and subsurface water storage capacities directly.

3.2.1 Comparison among herbaceous crops

Considering the events number for the whole period, independently from the runoff quantity, sorghum plots had the lowest number of events, as average among plots, while alfalfa had the highest number of events (Tab.4). This is mainly due to the rainfall characteristics, which substantially influence the runoff generation. In fact comparing the wettest (2005/06, with 997 mm) and the driest year (2006-07, with 496 mm), both occurring with alfalfa, the number of runoff events, as average of all the plots, was 23 and 3 respectively. Indeed, 2002-03 was another dry year (520mm) with the same coverage but it produced 16 runoff events. This difference with the 2006-07 year may be explained by the distribution of the rainfall events during the year: in 2002-03 all the events were during the fall-winter, apart from four in April, and were quite abundant, while in 2006-07 the few events were distributed more homogeneously during the whole year. Furthermore, of all these rainfall events, in 2002-03 there were 18 "heavy rains", while only 10 in 2006-07. So the different number of events of runoff to equal amounts of rain is, in this case, connected to its distribution throughout the year. A significant linear relationship between P (mm/year) and number of runoff events was found, with alfalfa as vegetation cover, independently from slope (Fig. 7), not taking into account the year 2002-03,
Having a higher number of runoff events with a multiannual crop, such as alfalfa and rye-grass (Tab. 4) may be due to a change of the crop cover during the years. In particular during the alfalfa years a variation of vegetation cover was visually observed and proved through the yield data. As shown in Fig. 8 the trend of its annual yield for 7 years has a bell-shape, highlighting that the soil cover was higher in the central period, while it was lower in the beginning and final periods. In the year 2002-03, the yield was 6,5 t/ha, as an average, with the largest number of event (16), while in 2006-07 it was 5.6 t/ha, with a very low number of events (4). These diverse yields may demonstrate a different effectiveness in protecting soil from runoff
In addition to the number of events, it is interesting to evaluate the amount of runoff measured. To determine runoff differences due to crop effects, the data set of the sub-period 1996-2002 was considered, i.e. three crop cycles of wheat, two of sorghum and three of

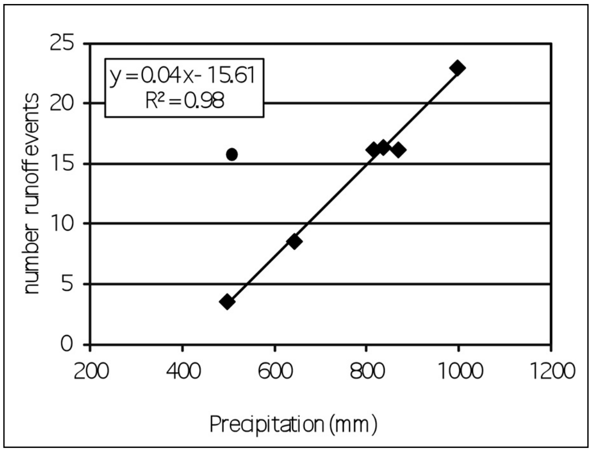

Fig. 7 - Runoff events number (mean of the plots) as a function of the annual precipitation in the period 2000-2007. The dot is the year 2002-03, and was not considered in the regression equation.
Fig. 7 - Numero di eventi di runoff (media delle parcelle) in funzione della pioggia annuale nel periodo 2000-2007. Il punto è dell'anno 2002-03 e non è considerato nell'equazione di regressione.

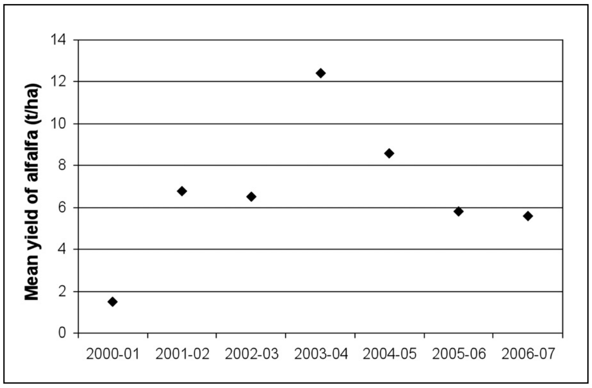

Fig. 8 - Alfalfa mean yield during the years (t/ha).
Fig. 8 - Rese medie dell'erba medica nel periodo studiato (t/ha).

alfalfa. The mean annual runoff was 0.8mm for wheat, 40.2mm for sorghum and 1.6mm for alfalfa. Indeed there was a high variability among years with the same crop, probably due to the diverse characteristics of the rainfall events which produced runoff.
Fig. 9 shows the mean monthly runoff quantities for the different crops. As it was highlighted also with the annual amount, the most abundant runoff events occurred with sorghum, when the soil was bare after harvesting and the rain plentiful (Oct-Dec), having runoff coefficients ranging from 0.01 to 0.81 mm per event, depending on plot and month. Wheat showed low runoff values the year around, having only one runoff event higher that 1 mm (in November, in plot O1, O2, and G). Alfalfa protected the soil better than the other crops, with the smallest quantity of yearly runoff. With alfalfa the highest monthly runoff was 6.7 mm in January; in the other rainy months runoff was quite small (<1 mm) in all plots.
This results can be explained by the diverse crop cycle: with sorghum the soil was bare for about eight months, mostly during the rainy seasons. The alfalfa has a permanent soil coverage for the whole year, while the other species left the soil bare for long periods (Bochet and García-Fayos, 2004).
In the sub-period 1996-2002, characterized by annual precipitation close to the climatic mean of the area, alfalfa and wheat were more effective than sorghum in limiting runoff. When looking at the number of runoff events (Tab. 4) alfalfa had the largest (13 as an average of the two years) followed by sorghum (8 events) and wheat (6 events) .

3.2.2 Comparison between alfalfa and cherry wood
Alfalfa and cherry wood are both multiannual crops, characterized by a full coverage of the soil for the whole year. Fig. 10 shows the runoff amount for all plots cultivated with alfalfa and cherry wood in five representative events, occurred during the crop cycle 2001/2002. No clear differences between alfalfa and cherry wood crops can be deduced from the graph, despite the higher slope of the C plot (17,9%) with respect to the others. Indeed, as reported also by several other studies (Sinun *et al.*, 1992; Wiersum, 1984) the canopies of orchards or forest are very effective in reducing the erosive power of raindrops and they provide materials for soil cover on the forest flow (Fang *et al.*, 2012). The interception of raindrops through trees canopy, underwood and litterfall lead to a reduction of the raindrop energy, which depends on the raindrops' size and velocity, to almost zero, when it reach the soil (Binkley and Brown, 1993). So the soil protection is guaranteed all the year: during the summer the foliage of cherries intercept the rainfall

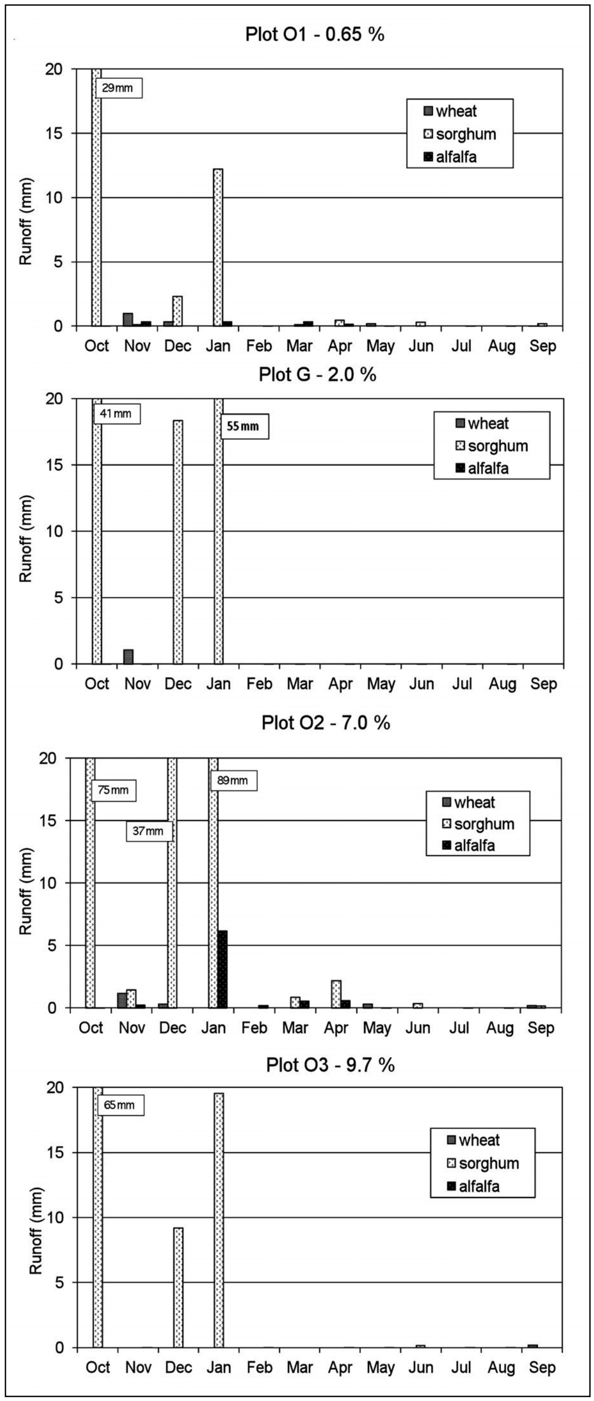

Fig. 9 - Average monthly runoff (mm) in plots O1, G, O2, O3 of the period 1996-2002.
Fig. 9 - Runoff medi mensili (mm) nelle parcelle O1, G, O2, O3 del periodo 1996-2002.

drops, while in autumn, despite the absence of foliage coverage, both the undergrowth and the leaves of the cherry trees, fallen on the ground, constitute a protective layer on the soil, absorbing the rainfall impact energy. Only in February the runoff generated in the C

Crop cycle	Crop	P (mm)	Number of runoff events					
			O1	G	O2	O3	R	mean
1992-93	Maize	861.4	12	12	11	12	12	***12***
1993-94	Wheat	930.2	16	16	16	16	16	*16*
1995-96	Wheat	752.0	13	13	13	13	13	*13*
1997-98	Wheat	500.0	3	3	3	3	3	*3*
1999-00	Wheat	709.0	3	3	3	3	3	*3*
	Mean	***723.9***	*9*	*9*	*9*	*9*	*9*	***9***
1994-95	Sorghum	798.5	8	8	8	8	8	*8*
1996-97	Sorghum	832.0	10	10	10	10	10	*10*
1998-99	Sorghum	619.4	5	5	5	5	5	*5*
	Mean	***749.9***	*8*	*8*	*8*	*8*	*8*	***8***
2000-01	Alfalfa	642.0	9	8	9	9	8	*9*
2001-02	Alfalfa	835.2	17	10	19	20	16	*16*
2002-03	Alfalfa	520.0	14	20	19	15	13	*16*
2003-04	Alfalfa	867.8	16	17	17	16	15	*16*
2004-05	Alfalfa	814.4	15	17	19	16	14	*16*
2005-06	Alfalfa	996.6	24	21	25	22	23	*23*
2006-07	Alfalfa	496.0	4	3	4	4	3	*4*
	Mean	***738.9***	*14*	*14*	*16*	*15*	*13*	***14***
2007-08	Rye-grass	594.6	14	8	13	14	14	*13*
2008-09	Rye-grass	894.6	12	7	14	13	13	*12*
	Mean	***744.6***	*13*	*8*	*14*	*14*	*14*	***12***

Tab. 4 - Crop, annual rainfall (mm) and number of runoff events for each crop cycle of the trial and its average per year.
Tab. 4 - Specie colturale, quantità di pioggia annuale (mm), numero di eventi di runoff per ciascun ciclo colturale e sua media annuale.

plot is higher than the other plots, apart from O2, and this can be explained considering that, in winter, trees are without leaves and the runoff is contrasted only by a reduced undergrowth.
In any case, in general the cherry wood plot, with its heterogeneous undergrowth, is able to control with efficacy the rainfall effect on runoff and erosion, for the whole year.

3.3 Relationship of slope and land modeling with runoff events

Tab.5 shows the values of the main characteristics of runoff (number of events, maximum and average amount of runoff per event, in mm) and the slope of the plots with herbaceous crops, in the period 1996-2002. (For plot R quantitative values were not available for that period).
The plot slope affects the maximum amount of runoff, but not the number of events or the average runoff. Considering the diagonal plots (O1, O2, O3), the average runoff is low in plots with low slope; for steep slopes the path length of water has the main influences on the phenomenon. In fact, as reported by Leys et al (2010) runoff and erosion are scale-dependent: the experimental plots have the same size (50m x 20m), but the runoff runs a path due to the tillage direction, up to convey to the downstream ditch. Furthermore, the length that the water takes depend on the plot

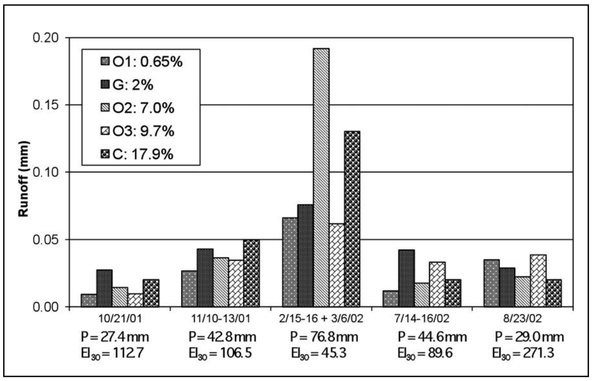

Fig. 10 - Runoff amount in the plots cultivated with alfalfa (O1, G, O2, O3) and cherry tree wood (C) in five representative events of the year 2001/02. In x-axis the date of the rainfall events, the precipitation amount and the EI_{30} are indicated.
Fig. 10 - Confronto tra cinque eventi di runoff rappresentativi avvenuti nel 2001/02, misurati nelle parcelle coltivate con erba medica (O1, G, O2, O3) e in quella con i ciliegi da legno. Nell'asse delle x vengono indicati: la data, la quantità e l'erosività EI_{30} dell'evento di pioggia.

modeling. Considering all the plots with herbaceous crops, for the entire period 1992-2009, the number of runoff events was maximum in plots diagonally ploughed (O1, O2 and O3) and minimum in the contour lines plot (G), as an average over the period, regardless to the crop (Tab. 5).
The effect of the land modeling is evident only for alfalfa and rye-grass, grown in the final period of the experiment. While, in fact, for the other crops the number of runoff events does not change depending on the plot, this does not happen for alfalfa and rye-grass. In particular the G and R plots reduce the runoff events of alfalfa with a percentage ranging from 6 to 17%, depending on the compared plot, while the G plot decreases the number of events with rye-grass of 45% (Tab. 4).

Plot	O1	G	O2	O3
Slope	0.65%	2.0%	7.0%	9.7%
N. runoff events	41	22	40	22
Mean runoff (mm/event)	2.1	8.8	9.4	8.1
Max runoff (mm/event)	58.2	81.0	143.4	128.9

Tab. 5 - Characteristics of runoff as a function of plot slope for the period 1996-2002.
Tab. 5 - Caratteristiche del runoff in funzione della pendenza delle parcelle nel periodo 1996-2002.

The effectiveness of the up-and-down plot (R) in limiting runoff events, over the years cultivated with alfalfa, is closely linked to soil texture. The sandy loam soil, together with the long path before reaching the ditches, enhances the infiltration of water through the soil instead of surface runoff.
Regarding to the effect of crops, annual crops (wheat and sorghum), determine as an average eight or nine events per year, while rye-grass can get to thirteen events per year, probably due to the low germination of this crop in summer arid conditions, that limit the coverage effect.

CONCLUSIONS

Slope, crop cover and land modeling affect the quality and quantity of runoff events, but the results obtained during a 17-year-long experiment show that rainfall has the greatest effect. In particular the rainfall amount and its picks are the most important factors in predicting and indicating the degree of runoff and soil erosion in the studied area. It's very important knowing the pluviometric regime of the studied area, since in the majority of events erosion depends on a few intense rainfall events.
Considering the land modeling, the contour plot resulted the most efficient in limiting runoff, followed by downslope, while the diagonally ploughed, independently by slope, can lead to many more events, indicating that the length of the path may have a inverse effect on soil conservation. Regarding to the effect of crops, annual crops (wheat and sorghum), determine as an average eight or nine events per year, while rye-grass can get to thirteen events per year, probably due to the low germination of this crop in summer arid conditions, that limits the coverage effect.
Between the permanent vegetation, good results are obtained with the cherry tree wood, with which the land is protected by the canopy and that, even with only the undergrowth, limits the surface runoff in comparison with the other perennial crop, alfalfa. The role of alfalfa seems to be controversial, a larger number of runoff events, but all of quite low amount and consequently only slightly erosive.

ACKNOWLEDGEMENTS

This research was possible thanks to financial support of the CNR (IPRA Project) and the Ministry of Education. We thank Dr. Rapparini for the support in the management of the trial, and Dr. Vignudelli for the realization of Fig. 2.

REFERENCES

Ampofo E.A., Muni R.K., Bonsu M. 2002. Estimation of soil losses within plots as affected by different

agricultural land management. Hydrol. Sci. J., 47(6): 957-967.
Baumhardt R.L., Jones O.R. 2002. Residue management and tillage effects on soil-water storage and grain yield of dryland wheat and sorghum for clay loam in Texas. Soil Tillage Res., 68: 71-82.
Binkley D., Brown T.C., 1993. Management Impacts on Water Quality of Forests and Rangelands. Gen. Tech. Rep. RM-239. USDA Forest Service, Fort Collins.
Bochet E., García-Fayos P., 2004. Factors Controlling Vegetation Establishment and Water Erosion on Motorway Slopes in Valencia, Spain. Restoration ecology 12 (2), 166-174.
Desmet P.J.J., Govers G. 1997. Two-dimensional modeling of the within-field variation in rill and gully geometry and location related to topography. Catena., 29: 283-306.
Fang N., Shi Z., Li L., Guo Z., Liu Q., Ai L., 2012. The effects of rainfall regimes and land use changes on runoff and soil loss in a small mountainous watershed. Catena, 99:1-8.
Fisher R.A., Santiveri F., Vidal I.R. 2002. Crop rotation, tillage and crop residue management for wheat and maize in sub-humid tropical highlands. Field Crops Res., 79: 123-137.
Grace J.M. 2002. Effectivness of vegetation in erosion control from forest road sideslopes. Trans. ASAE., 45(3): 681-685.
Leys A., Govers G., Gillijins K., Berckmoes E., Takken I. 2010. Scale effect on runoff and erosion losses from arable land under conservation and conventional tillage: the role of residual cover. J. Hydrol., 390: 143-154.
Ludwing B., Boiffin J., Chadoeuf J. Auzet A.V. 1995. Hydrological structure and erosion damage caused by concentrated flow in cultivated catchments. Catena., 25: 227-252.
Luino F. 2005. Sequence of instability processes triggered by heavy rainfall in the northern Italy. Geomorphology, 66:13-39.
Nadal-Romero E., Regüés D., Latron J., 2008. Relationships among rainfall, runoff, and suspended sediment in a small catchment with badlands. Catena 74, 127-136.
Pieri L., Bittelli M, Hanuskova M., Ventura F., Vicari A., Rossi Pisa P., 2009. Characteristics of eroded sediments from soil under wheat and maize in the North Italian Apennines. Geoderma 154, 20-29.
Romkens M.J.M., Helming K. Prasad S.N. 2001. Soil erosion under different rainfall intensities, surface roughness and soil water regimes. Catena., 46: 103-123.
Rossi M., Vicari A., Gaspari N., Rossi Pisa P., Catizone P. 2000. Effetti della coltura e della modalità di lavorazione del terreno sull'erosione e sulla qualità delle acque di ruscellamento. Riv. Agron., 34: 352-363.
Rossi Pisa P., Ardizzoni E., Gaspari N., Pagliai M. 1986. Effetti di diverse direzioni di lavorazione su alcune caratteristiche fisiche di terreni in pendio. Riv, Agr., 20: 2-3, 329-335.
Rossi Pisa P., Ventura F., Gaspari N., Ardizzoni E. 1996. Effetto della sistemazione dei terreni e dell'avvicendamento colturale sull'erosione in zone agrarie in pendio. Proceedings of Convegno scientifico in occasione del triennale dell'alluvione di Firenze "La difesa dalle alluvioni", Firenze pp. 473-482.
Rossi Pisa P., Ventura F., Vicari A., Vitali G. 1999. Land use effects on runoff at watershed and field scale. Proceedings of the 3th GCTE Focus Conference "Food & Forestry, Global Change and Global Challenges", Reading, UK p. 105.
Sinun W., Meng W.W., Douglas I., Spencer T., 1992. Throughfall, stemflow, overland flow and throughflow in the Ulu Segama rain forest, Sabah, Malaysia. Philosophical Transactions of the Royal Society 335, 389-395.
Souchère V., King D., Daroussin J., Papy F. 1998. Effect of tillage on runoff directions, consequences on runoff contributing area within agricultural catchments. J. Hydrol., 206: 256-267.
Takken I., Jetten V., Govers G., Nachtergaele J., Steengen A. 2001a. The effect of tillage-induced roughness on runoff and erosion patterns. Geomorphology., 37:1-14.
Takken, I., Govers, G., Steegen A., Nachtergaele, J., Guérif, J., 2001b. The prediction of runoff flow directions on tilled fields. J. Hydrol., 248: 1-13.
Ventura F., Rossi Pisa P., Vicari A., 2004. Effect of land use on soil erosion in a small watershed of Emilia Romagna region. Italian Journal of Agronomy, 8, 1, 29-36.
Wiersum K.F., 1984. Surface erosion under various tropical agroforestry systems. In: O'Loughlin, C.L., Pearce, A.J. (Eds.), Proceedings of the Symposium on the Effects of Land Use on Erosion and Slope Stability. Honolulu, May 1984, pp. 231-239.
Wischmeier W.H., Smith D.D. 1978. Predicting rainfall erosion losses. A guide to conservation planning. U.S. Department of Agricultural, Agricultural Handbook n. 537.
Zhang X-CJ., Garbrecht J.D. 2002. Precipitation retention and soil erosion under varying climate, land use, tillage and cropping system. J. Am. Water Resour. Assoc., 38: 1241-1253.

Analysis of the Climatic Aggressiveness of Rainfall in the Abruzzo Region

Bruno Di Lena[1], Fernando Antenucci[1], Lorenzo Vergni[3], Luigi Mariani[2]*

Abstract: *The aim of this paper has been to describe the space and time behavior of the climatic aggressiveness of rainfall in the Abruzzo region by means of the Modified Fournier Index (MFI). A preliminary evaluation of the MFI reliability has been performed by comparing the mean MFI with the corresponding RUSLE rainfall-runoff erosivity factor (R) at 9 stations for which rainfall data at 15-minute time steps are available. Afterwards, the spatial variability of MFI was investigated using an ordinary Kriging. The temporal variability has been studied evaluating the slope and the significance of trends in the MFI time series. Results show that the region of Abruzzo can be subdivided in 3 spatially coherent zones, characterized by different levels of climatic aggressiveness of rainfall: area with low aggressiveness (endo-mountain area ad coastal area with low yearly rainfall) and area with medium aggressiveness (mountain areas with abundant precipitation) which embeds some spots with high aggressiveness. Time behavior shows a decline of the climatic aggressiveness which can be attributed to the new climatic phase that affects the Euro-Mediterranean area from the 90's of the twentieth century.*

Keywords: *MFI index, Abruzzo, temporary and spatial variability.*

Riassunto: *Scopo della ricerca è stato quello di descrivere, con riferimento al territorio abruzzese, la variabilità spazio temporale dell'aggressività climatica della pioggia descritta per mezzo del Modified Fournier Index (MFI). L'attendibilità di tale indice è stata preliminarmente valutata confrontando i valori medi di MFI con i corrispondenti valori del fattore di erosività della pioggia (R) della RUSLE, quantificati in 9 stazioni per le quali erano disponibili dati di precipitazione a 15 minuti. La variabilità spaziale di MFI è stata quindi indagata tramite un Kriging ordinario. La variabilità temporale è stata studiata valutando intensità e significatività dei trend nelle serie di MFI. I risultati ottenuti mostrano che a livello spaziale il territorio regionale è suddivisibile in 3 zone spazialmente coerenti, caratterizzate da diversi livelli di aggressività climatica della pioggia: una zona a bassa aggressività (areale costiero ed areale endo-montano a più bassa piovosità) ed una a media aggressività (aree montane più piovose). In queste ultime si evidenziano alcune zone con elevati valori di aggressività. A livello temporale si evidenzia una generale riduzione dell'aggressività climatica della pioggia che potrebbe essere associato alla nuova fase climatica che interessa l'area euro-mediterranea dagli anni 90 del XX secolo.*

Parole chiave: *indice MFI, Abruzzo, variabilità spaziale e temporale.*

INTRODUCTION

Soil erosion is a complex phenomenon driven by many factors such as climate, soil physical characteristics, slope and slope length, vegetation cover, and tillage system. With regard to the climate, it is essential to evaluate the rainfall aggressivity on soil (erosivity) which depends on rainfall amount and intensity.

Different indices of erosivity have been proposed and the most appropriate ones seem to be those relating soil erosion with kinetic energy of rainfall, such as the well-known EI_{30} (Wischmeier, 1959, Renard et al., 1997). However for the calculation of EI_{30} there is usually scarce availability of high quality datasets on a regional scale, because rainfall data at a small time step are required. Fort this reason, other indices have been proposed based on hourly maximum rainfall intensity with a given return time (Renard and Freimund, 1994; Lo et al., 1985) or based on daily rainfall (Bagarello and D'Asaro, 1994). Furthermore, the Fournier index (Fournier, 1960) was modified by Arnoldus (1980) to obtain the MFI index which can be applied when only monthly data are available. MFI index calculation is based on the ratio between the sum of the squared monthly precipitation and the total yearly precipitation. According to this index, for a given total yearly rainfall an higher erosivity is observed when rainfall events are concentrated on brief periods along the year.

Literature provides several examples of the use of MFI as simplified index for the evaluation of the rainfall aggressiveness. Ferro et al., (1991) studying

* Corresponding Author e-mail: dilenab@arssa-mail.it
[1] Regione Abruzzo- Direzione Politiche Agricole e di Sviluppo Rurale
[2] Università degli studi di Milano - DISAA
[3] Università degli studi di Perugia - Dipartimento di Ingegneria Civile ed Ambientale
Received 24 July, accepted 20 October 2012.

the spatial variability of erosivity in Sicily, showed an evident correlation between MFI and EI_{30}. Gregori et al. (2006), on 292 Italian stations, observed a close relationship between the MFI and other simplified indices of aggressiveness (such as the highest rainfall recorded in intervals of 6 and 24 hours for a return period of 2 years).

The European project CORINE (Coordination of Information on the Environment) adopted both the MFI index and the Gaussen Bagnolus aridity index in order to the determine an index of climatic erosivity, which is useful to assess the potential and current risk of erosion (CORINE,1995).

Taguas et al (2011), in the light of the good relationship between the calculated rainfall erosivity recorded every 10 minutes for a period of three years and the one defined by the MFI, have used this later to analyze the erosivity of rainfall in southern Spain.

Deyanira and Donald (2005) found a good relationship between the MFI obtained for different areas of Venezuela and the erosivity factor of the USLE model (Wischemeier and Smith, 1978).

The MFI has also been recently applied by De Luis et al., (2010) which evaluated the long-term trends of the rainfall erosivity in the Iberian Peninsula.

This paper analyzes rainfall erosivity by the MFI, in 75 locations in the Abruzzo region evenly distributed over the territory, for the period 1951-2009. The purposes of this analysis are to: identify the homogeneous areas in terms of MFI and highlight the possible presence of trends in MFI during the examined period.

DATA AND METHODS

The study was carried out using the monthly rainfall data collected by the Hydrographic Service of the Abruzzo region for the reference period 1951-2009 in 75 stations which show a percentage of missing data less than 10% and are evenly distributed over the territory (Fig. 1).

Missing data were reconstructed from the data of stations with a distance of less than 20 km (Vergni *et al.*, 2009) and adopting the technique of weighted average with weight inversely proportional to the square of the distance (Wei and Mc Guinness, 1973).

The index MFI for each station and for each year was calculated with the following formula:

$$MFI = \sum_{1}^{12} \left(\frac{p^2}{P} \right)$$

where p (mm) is monthly precipitation and P (mm) is the yearly precipitation.

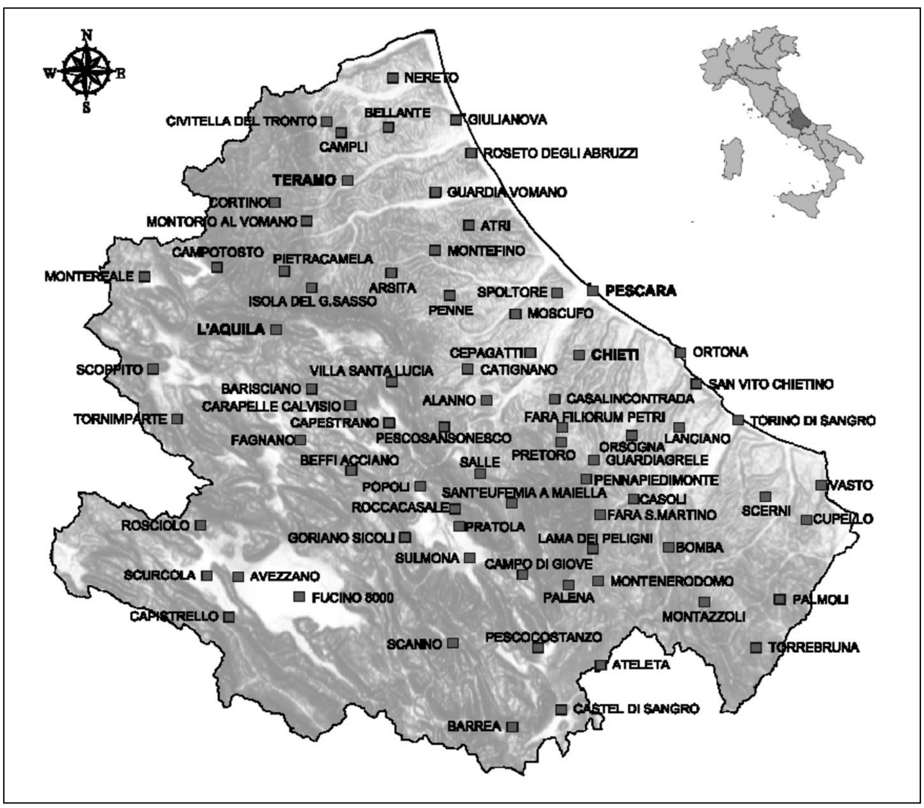

Fig. 1 - Location of stations used for this study.
Fig. 1 - Posizione delle stazioni usate in questo studio.

Class	Description
low	MFI<100
intermediate	100≤MFI<150
high	MFI ≥150

Tab. 1 - MFI index classification.
Tab. 1 - Classificazione dell'indice MFI.

It is interesting to observe that MFI can be also computed as a function of the Precipitation Concentration Index (PCI; Olivier, 1980)

$$PCI = \frac{\sum_{1}^{12} p^2}{\left(\sum_{1}^{12} p\right)^2}$$

$$MFI = PCI \cdot P$$

According to this relationship, rainfall aggressiveness by MFI is higher where there are high values of precipitation concentration (high seasonality, high PCI) and/or total annual precipitation (P).
Climatic aggressiveness of rainfall has been interpreted adopting the classes listed in table 1 (Gregori *et al.*, 2006).
The trend analysis over the reference period has been carried out applying the Mann-Kendall non parametric test on cumulative annual rainfall and MFI index (Mann, 1945; Kendall, 1975).
The absence of trends in the population from which the dataset under investigation has been extracted is the null hypothesis (H0) of the Mann-Kendall test. According to the alternative hypothesis, however, it is true that the series analyzed have a positive or negative trend.
Assuming H0 as true, the standard value (Z_s) of the test statistic calculated on Kendall's series, has a probability (p-value) given by:

$$p\text{-value} = 2\left[1 - \phi|Z_s|\right]$$

Where ϕ is the cumulative probability function of a standard normal distribution. It follows that the decrease of p-value (less than a certain significance level) increases the evidence of the presence of trends (rejection of H0). In the present paper a p-value <0.10 was considered significant. The Mann-Kendall test can detect the existence of a monotonic trend, but does not allow its measurement. For this reason the nonparametric Theil-Sen estimator (Theil, 1950; Sen, 1968) has been adopted to estimate the slope (β) of the straight lines interpolating the data.
The *Kendall* and *Zyp* libraries of the R statistical software have been adopted respectively for the calculus of the Mann-kendall test and the Theil-Sen estimator.
The detection of areas affected by significant trends (decreasing or increasing), associated with high levels of confidence (p-value <0.10), was obtained by interpolating punctual p-values of the Mann-Kendall test with the technique of Ordinary Kriging. The maps has been produced with the version 7 of the Surfer software.

EVALUATION OF THE MFI RELIABILITY

The use of the MFI in the quantification of the rainfall erosivity has been analyzed and verified by many authors (Arnoldus, 1980; Ferro *et al.*, 1991; Coutinho and Tomas, 1994). In this paper a further evaluation (not exhaustive, due the limited available dataset) of the MFI index is performed. At this end, the best term of comparison is the rainfall erosivity factor R (MJ mm ha^{-1} h^{-1} year^{-1}) of the revised universal soil loss equation (RUSLE) generally considered as one of the best parameters to quantify rainfall erosivity. Following the procedure suggested by the more recent RUSLE erosion modelling framework (Renard *et al.*, 1997), R can be calculated as follows:

$$R = \frac{1}{n}\sum_{j=1}^{n}\left[\sum_{k=1}^{m}(E_k \cdot I_{30,k})\right]$$

where E_k (MJ ha^{-1}) and $I_{30,k}$ (mm h^{-1}) are respectively the total storm kinetic energy and the maximum 30-minute rainfall intensity of the kth storm, m is the number of storms in each year, n is the number of years used to obtain the average R. The product $E_k I_{30,k}$ or simply EI_{30} (MJ mm ha^{-1} h^{-1}) is the erosivity associated to each storm. Single storms are rainfall periods separated from other rain periods by more than 6 hours with no precipitation.
The total storm kinetic energy is quantified by:

$$E_k = \sum_{r=1}^{T} e_r \cdot \Delta V_r$$

where e_r is the rainfall energy per unit depth of area per unit area (MJ ha^{-1} mm^{-1}) and DV_r is the depth of rainfall (mm) for the rth increment (of duration t_r) of the storm hyetograph which is divided in T parts (each part is assumed to have constant intensity).
The rainfall energy per unit depth of rainfall (e_r, MJ

ha^{-1} mm^{-1}) is quantified by the equation of Brown and Foster (1987):

$$e_r = 0.29\left(1 - 0.72e^{-0.05 I_r}\right)$$

where the rainfall intensity can be computed as $I_r = \Delta V_r / t_r$ (mm h^{-1}).
The R calculation requires the availability of hyetograms, at least at 30-minute time step.
In the recent decades, several meteorological stations of the Abruzzo region were instrumented to provide data at 15-minute time step. Among these stations, 9 were selected (Arsita, Bomba, Caramanico Terme, Catignano, L'Aquila, Pescara, Sulmona, Teramo and Vasto) taking into account the data quality (completeness) and ensuring an acceptable area coverage of the region (Fig. 2). The data available for the time series 2002-2009 were used for the comparison between the mean MFI index and the R factor, as shown in Fig. 3.
The agreement (R^2=0.80) between the mean values of the two indices is satisfactory, taking into account the simplicity of the MFI index. Also the accuracy of the obtained model can be considered acceptable, being the Absolute Percentage Error (MAPE) and the Root Mean Square Error (RMSE) 17% and 232.8 MJ·mm·ha^{-1}·h^{-1}·year^{-1} respectively. At any rate, the validity and the applicability of the model is limited to the period and to MFI range on which the relationship has been derived. Furthermore a longer time series of R values would make it possible to perform both the calibration and the validation of the model splitting the series in two distinct datasets.

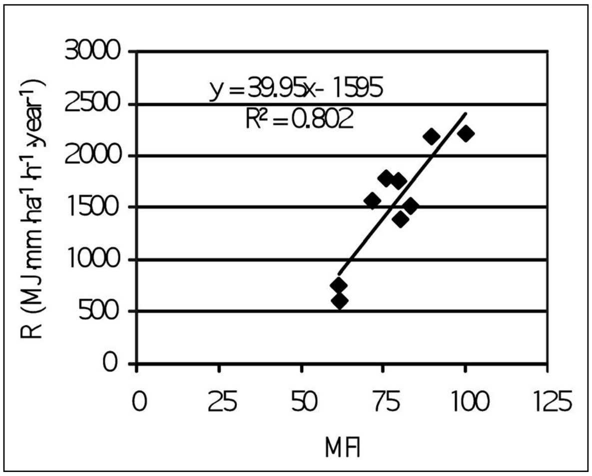

Fig. 3 - Comparison between the mean values of Modified Fournier Index (MFI) and of rainfall erosivity factor (R) computed with regards to 9 stations and a 9-year time series.
Fig. 3 - Confronto fra i valori medi del Modified Fournier Index (MFI) e del fattore di aggressività della pioggia (R) riferiti a serie novennali di nove stazioni.

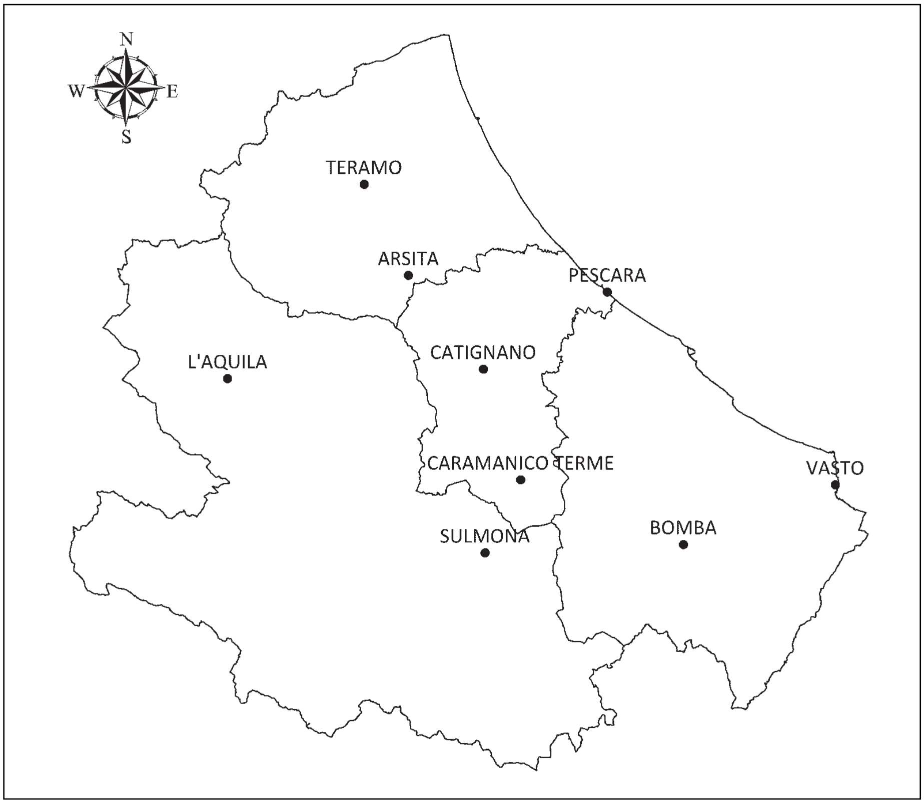

Fig. 2 - Stations used for the comparison between the R-factor of RUSLE and the index MFI.
Fig. 2 - Stazioni utilizzate per il confronto tra il fattore R della RUSLE e l'indice MFI.

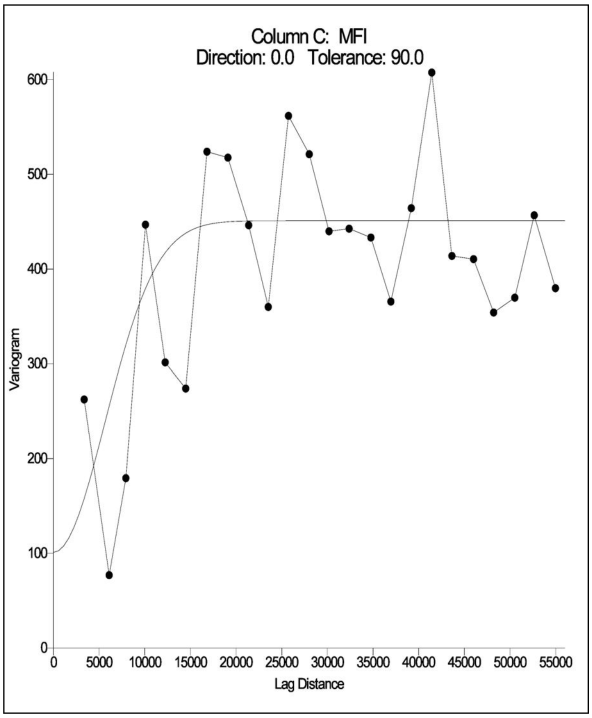

Fig. 4 - Semivariogram of MFI data. A spherical model with nugget=100, sill=350 and range=8000 has been adopted.
Fig. 4 - Semivariogramma dei dati dell'indice MFI. È stato adottato il modello sferico con nugget =100, sill=350 e range=8000.

RESULTS AND DISCUSSION

A preliminary approach to the relationship between yearly rainfall and MFI has been carried out analyzing the spatial behavior of the mean values. For this purpose the ordinary Kriging technique has been adopted preceded by the analysis of the experimental semivariogram followed by the adoption of a gaussian variogram model (Fig. 4). The map of yearly mean precipitation has been already presented and discussed (Di Lena *et al.*, 2012). Therefore, only the map of the mean yearly MFI for the period 1951-2009 (mean MFI values) is here presented (Fig. 5).

The climatic aggressiveness of rainfall is more considerable in areas at higher altitude characterized by higher yearly rainfall. On the other hand, a lower rainfall aggressiveness, stated by lower values of MFI below 100, can be appreciated for areas with lower yearly rainfall and more specifically:

– the central areas of the province of Aquila, where significant foehn-stau regimes give rise to a strong endo-mountain effect (Di Lena *et al.*, 2012).
– the coastal area, where there isn't the enhancing effect on rainfall due to the relief and local maxima are only due to the abrupt roughness increase in correspondence with the sea-land transition (Andersson, 1981).

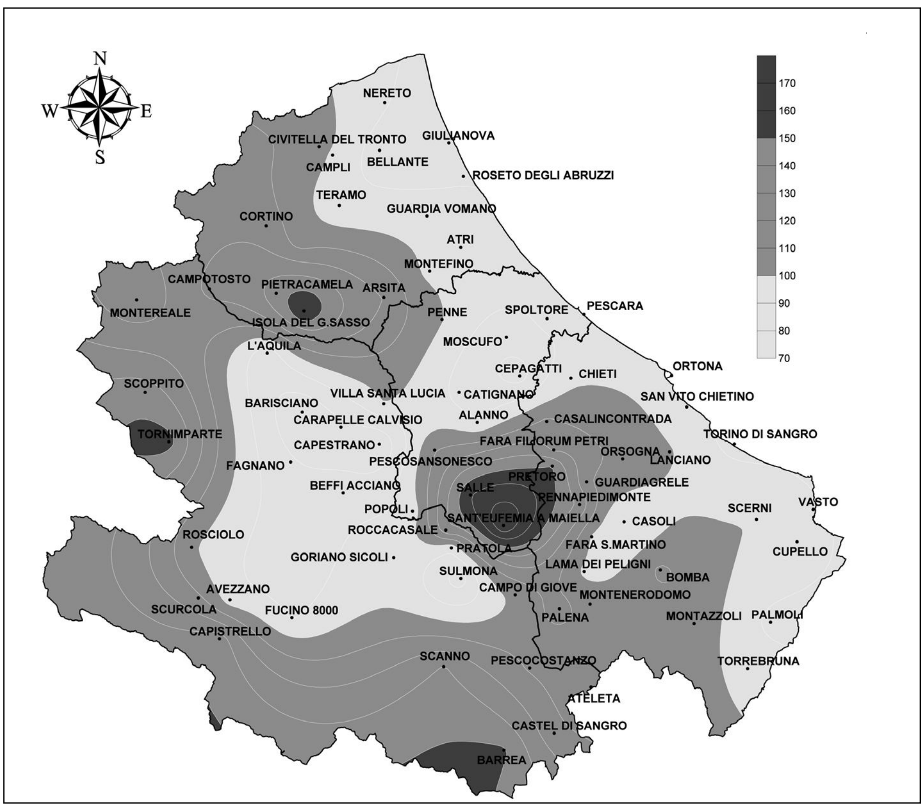

Fig. 5 - Map of the mean MFI values for Abruzzo region for the 1951-2009 period.
Fig. 5 - Mappa dei valori medi di MFI per la regione Abruzzo per il periodo 1951-2009.

BASIN	*STATION*	*Mean*	*Min*	*Max*	*C.V.*	*Erosivity class*
Pescocostanzo highland	PESCOCOSTANZO	108.9	54.5	160.0	20.0	intermediate
Aterno-Pescara	ALANNO	91.0	54.7	147.4	21.6	low
Aterno-Pescara	BARISCIANO	71.9	38.6	149.1	23.9	low
Aterno-Pescara	BEFFI ACCIANO	87.6	44.2	183.3	28.8	low
Aterno-Pescara	CAMPO DI GIOVE	102.0	51.8	150.3	21.1	intermediate
Aterno-Pescara	CAPESTRANO	70.0	35.2	109.4	24.1	low
Aterno-Pescara	CARAPELLE CALVISIO	77.6	49.2	114.6	21.6	low
Aterno-Pescara	CASALINCONTRADA	112.1	76.4	178.3	21.5	intermediate
Aterno-Pescara	CATIGNANO	87.1	54.7	153.9	23.9	low
Aterno-Pescara	CEPAGATTI	76.0	53.7	115.3	19.6	low
Aterno-Pescara	CHIETI	97.8	61.7	156.5	19.9	low
Aterno-Pescara	FAGNANO	81.2	44.0	125.2	22.1	low
Aterno-Pescara	GORIANO SICOLI	99.6	49.2	157.4	26.5	low
Aterno-Pescara	L'AQUILA	82.6	47.4	111.5	20.3	low
Aterno-Pescara	MONTEREALE	101.7	61.1	139.5	19.6	intermediate
Aterno-Pescara	PESCARA	90.6	45.6	170.7	27.1	low
Aterno-Pescara	PESCOSANSONESCO	109.4	69.6	208.5	26.5	intermediate
Aterno-Pescara	POPOLI	94.2	47.7	196.0	28.9	low
Aterno-Pescara	PRATOLA	92.4	55.0	165.7	24.2	low
Aterno-Pescara	ROCCACASALE	126.7	65.8	341.4	38.5	intermediate
Aterno-Pescara	SALLE	149.7	94.3	260.9	21.8	intermediate
Aterno-Pescara	SANT'EUFEMIA A MAIELLA	169.5	89.4	280.2	21.8	high
Aterno-Pescara	SCANNO	130.7	65.8	226.8	24.1	intermediate
Aterno-Pescara	SCOPPITO	135.2	77.7	206.7	24.0	low
Aterno-Pescara	SPOLTORE	92.7	62.9	163.1	22.6	low
Aterno-Pescara	SULMONA	75.2	53.3	123.5	18.4	low
Aterno-Pescara	TORNIMPARTE	143.5	58.2	228.7	26.2	intermediate
Aterno-Pescara	VILLA SANTA LUCIA	100.1	51.8	205.4	30.1	intermediate
Feltrino	LANCIANO	101.0	60.3	177.3	24.4	intermediate
Feltrino	SAN VITO CHIETINO	91.6	40.9	193.0	26.5	low
Foro	FARA FILIORUM PETRI	118.0	65.7	221.3	21.4	intermediate
Foro	GUARDIAGRELE	111.6	50.8	204.9	27.2	intermediate
Foro	PRETORO	140.8	82.0	237.2	22.5	intermediate
LIRI at the confluence of the Fucino emissary	AVEZZANO	95.0	44.3	136.7	26.2	low
LIRI at the confluence of the Fucino emissary	CAPISTRELLO	135.7	60.9	269.3	29.4	intermediate
LIRI at the confluence of the Fucino emissary	SAN BENEDETTO DEI MARSI - FUCINO 8000	89.1	44.2	131.9	23.3	low
Moro	ORSOGNA	108.8	64.7	203.2	25.4	intermediate
Piomba	ATRI	99.5	39.2	183.7	31.7	low
Saline	ARSITA	119.7	57.9	189.1	24.8	intermediate
Saline	MONTEFINO	97.0	61.2	133.8	19.7	low
Saline	MOSCUFO	83.9	46.8	133.0	22.1	low
Saline	PENNE	100.5	58.1	163.8	21.3	intermediate
Salinello	CIVITELLA DEL TRONTO	108.6	51.6	199.4	27.6	intermediate
Sangro	ATELETA	100.9	48.7	145.1	19.4	intermediate
Sangro	BARREA	141.2	80.1	254.4	27.5	intermediate
Sangro	BOMBA	111.9	58.1	230.0	28.4	intermediate
Sangro	CASOLI	89.2	42.6	160.0	27.8	low

follows

continue

BASIN	*STATION*	*Mean*	*Min*	*Max*	*C.V.*	*Erosivity class*
Sangro	CASTEL DI SANGRO	113.4	58.6	177.8	21.8	intermediate
Sangro	FARA SAN MARTINO	99.0	59.7	177.3	26.1	low
Sangro	LAMA DEI PELIGNI	98.0	54.9	160.7	25.4	low
Sangro	MONTENERODOMO	105.7	63.5	152.8	20.2	intermediate
Sangro	PALENA	113.5	59.1	157.7	19.3	intermediate
Sangro	PENNAPIEDIMONTE	128.0	75.4	224.4	23.4	intermediate
Sinello	CUPELLO	93.8	39.5	208.5	34.0	low
Sinello	MONTAZZOLI	105.3	56.9	177.3	20.3	intermediate
Sinello	SCERNI	99.8	64.5	176.1	26.6	low
Tevere (Zona VIII) Nera	ROSCIOLO	101.5	50.3	166.3	25.2	intermediate
Tevere (Zona VIII) Nera	SCURCOLA MARSICANA	112.1	52.5	188.2	25.6	intermediate
Tordino	BELLANTE	86.3	49.2	139.6	24.9	low
Tordino	CAMPLI	96.8	45.4	144.1	24.5	low
Tordino	CORTINO	116.0	65.1	188.9	25.0	intermediate
Tordino	TERAMO	92.6	55.9	143.1	22.7	low
Trigno	PALMOLI	87.4	45.1	187.0	28.9	low
Trigno	TORREBRUNA	97.3	47.4	159.0	23.4	low
various	GIULIANOVA	82.2	48.3	152.5	27.8	low
various	ORTONA	94.3	44.9	216.9	30.4	low
various	ROSETO	88.7	52.9	143.9	25.5	low
various	TORINO DI SANGRO	86.9	47.4	193.7	27.0	low
various	VASTO	90.9	43.3	179.5	28.4	low
Vibrata	NERETO	90.8	42.0	167.5	29.3	low
Vomano	CAMPOTOSTO	122.4	84.1	171.6	18.4	intermediate
Vomano	GUARDIA VOMANO	94.7	55.6	165.1	24.6	low
Vomano	ISOLA DEL GRAN SASSO	151.7	79.4	253.0	22.9	high
Vomano	MONTORIO AL VOMANO	105.8	68.4	170.6	22.3	intermediate
Vomano	PIETRACAMELA	135.9	65.5	214.6	26.5	intermediate

Tab. 2 - Descriptive statistics of the MFI index.
Tab. 2 - Statistiche descrittive dell'indice MFI.

Following the criteria of table 1, it can be stated that the climatic erosivity of rainfall is low in 40 localities (53.3% of the total), medium in 33 (44.0%) and high in 2 (2.6%) with the maximum at Sant'Eufemia a Maiella (169.5) and the minimum at Barisciano (70). The coefficient of variability, which describes the data dispersion around the mean, reaches its maximum at Roccacasale (38.5%) and its minimum at Sulmona (18.4%) (Tab. 2).
The trend analysis highlights that the MFI index is decreasing in 63 locations representing 84% of the total, with an average slope β of -0.307 units / year. The MFI index is rising at 12 sites with an average slope β of 0.157 units / year. The increasing trend was significant only at the station of Tornimparte where the slope β is 0.667 units / year (Tab. 3).
The decrease is closely correlated, as expected, with the trend in cumulative annual rainfall (Tab. 3). The downward trends are significant only in 27 stations with an average slope of β -0.500 units / year. In most cases, the significant decrease in MFI index has a correspondence in the decrease of cumulative annual rainfall.
Some exceptions are the stations of Chieti, Pescara, Pratola Peligna, Fara Filiorum Petri and Pennapiedimonte where the significant decrease of annual rainfall didn't cause a significant decrease of MFI. Furhtermore, a significant decline of the MFI has been found in the location of Beffi Acciano, although the same has not been affected by a significant decrease of annual rainfall. These conditions could be attributed to the monthly distribution of rainfall that has remained unchanged, balancing or reducing the effect of the decreasing trend in the cumulated rainfall. At any rate it is evident that, under the typical climatic

HYDROGRAPHIC BASIN	*STATION*	*MFI index*		*Yearly cumulated precipitation*	
		β	Sign.	*β*	Sign.
Pescocostanzo highland	PESCOCOSTANZO	**-0,471**	**	**-3,145**	*
Aterno-Pescara	ALANNO	0,111	ns	0,279	ns
	BARISCIANO	-0,121	ns	-0,571	ns
	BEFFI ACCIANO	**-0,327**	+	-1,708	ns
	CAMPO DI GIOVE	-0,047	ns	0,628	ns
	CAPESTRANO	-0,063	ns	0,565	ns
	CARAPELLE CALVISIO	-0,091	ns	-0,041	ns
	CASALINCONTRADA	-0,105	ns	-1,713	ns
	CATIGNANO	0,167	ns	1,060	ns
	CEPAGATTI	**-0,250**	*	**-3,071**	**
	CHIETI	-0,150	ns	**-2,300**	+
	FAGNANO	**-0,350**	*	**-1,663**	+
	GORIANO SICOLI	**-0,727**	**	**-4,781**	**
	L'AQUILA	**-0,333**	*	**-2,194**	*
	MONTEREALE	0,073	ns	1,450	ns
	PESCARA	-0,280	ns	**-3,462**	*
	PESCOSANSONESCO	**-0,696**	***	**-5,800**	***
	POPOLI	**-0,476**	*	**-2,855**	*
	PRATOLA	-0,133	ns	-1,988	+
	ROCCACASALE	-0,286	ns	-3,161	ns
	SALLE	-0,269	ns	-1,853	ns
	SANT'EUFEMIA A MAIELLA	**-0,846**	**	**-4,185**	+
	SCANNO	**-0,636**	**	**-4,239**	*
	SCOPPITO	-0,130	ns	-1,438	ns
	SPOLTORE	**-0,333**	*	**-4,150**	***
	SULMONA	-0,080	ns	-0,867	ns
	TORNIMPARTE	**0,667**	*	**5,725**	**
	VILLA SANTA LUCIA	**-0,429**	+	**-2,765**	+
Feltrino	LANCIANO	**-0,333**	+	**-3,305**	**
	SAN VITO CHIETINO	**-0,378**	*	**-3,974**	**
Foro	FARA FILIORUM PETRI	-0,250	ns	**-3,000**	*
	GUARDIAGRELE	**-0,396**	+	**-4,367**	*
	PRETORO	**-0,757**	***	**-7,179**	***
LIRI at the confluence of the Fucino emissary	AVEZZANO	-0,200	ns	0,383	ns
	CAPISTRELLO	**-0,775**	*	**-5,522**	**
	SAN BENEDETTO DEI	**-0,348**	*	**-2,190**	+
	MARSI - FUCINO 8000				
Moro	ORSOGNA	-0,222	ns	-2,254	ns
Piomba	ATRI	-0,069	ns	-3,000	ns

follows

continue

HYDROGRAPHIC BASIN	*STATION*	*MFI index*		*Yearly cumulated precipitation*	
		β	Sign.	*β*	Sign.
Saline	ARSITA	**-0,500**	*	**-3,424**	+
	MONTEFINO	-0,070	ns	-1,690	ns
	MOSCUFO	0,047	ns	-0,565	ns
	PENNE	0,068	ns	0,310	ns
Salinello	CIVITELLA DEL TRONTO	**-0,786**	***	**-6,400**	***
Sangro	ATELETA	-0,200	ns	-0,939	ns
	BARREA	-0,417	ns	-1,178	ns
	BOMBA	-0,111	ns	-2,022	ns
	CASOLI	-0,230	ns	-1,400	ns
	CASTEL DI SANGRO	**-0,542**	**	**-2,941**	*
	FARA SAN MARTINO	0,160	ns	0,855	ns
	LAMA DEI PELIGNI	-0,284	ns	-1,520	ns
	MONTENERODOMO	-0,297	ns	-1,210	ns
	PALENA	-0,111	ns	-0,620	ns
	PENNAPIEDIMONTE	-0,348	ns	**-4,877**	*
Sinello	CUPELLO	**-0,478**	+	**-5,134**	**
	MONTAZZOLI	0,114	ns	1,110	ns
	SCERNI	-0,032	ns	-0,550	ns
Tevere (Zona VIII) Nera	ROSCIOLO	**-0,357**	+	-1,155	ns
	SCURCOLA MARSICANA	0,055	ns	1,321	ns
Tordino	BELLANTE	-0,048	ns	-0,887	ns
	CAMPLI	**-0,422**	*	**-4,078**	**
	CORTINO	**-0,765**	***	**-6,633**	***
	TERAMO	-0,220	ns	-2,200	+
Trigno	PALMOLI	-0,038	ns	-0,793	ns
	TORREBRUNA	-0,192	ns	-1,975	ns
Various	GIULIANOVA	-0,173	ns	-2,000	ns
	ORTONA	-0,075	ns	-0,521	ns
	ROSETO	-0,143	ns	-1,629	ns
	TORINO DI SANGRO	-0,200	ns	**-2,250**	*
	VASTO	-0,001	ns	-0,893	ns
Vibrata	NERETO	**-0,353**	+	**-4,325**	**
Vomano	CAMPOTOSTO	0,229	ns	**3,633**	*
	GUARDIA VOMANO	0,050	ns	-0,918	ns
	ISOLA DEL GRAN SASSO	0,143	ns	2,088	ns
	MONTORIO AL VOMANO	**-0,425**	**	**-3,041**	*
	PIETRACAMELA	-0,156	ns	0,512	ns

Tab. 3 - Results of the Mann-Kendall test applied to the MFI index and to the yearly mean precipitation (ns = not significant, + P0.10, * P0.05, ** P0.01, *** P0.001). Significant trends are shown in bold.

*Tab. 3 - Risultati del test di Man-kendall applicato all'indice MFI e alle precipitazioni medie annue. (ns = non significativo, + P0.10, * P0.05, ** P0.01, *** P0.001). In neretto sono riportati i trend significativi.*

conditions of the Abruzzo region, the MFI is mainly affected by the total precipitation amount. In different climatic conditions, characterized by a very marked seasonality, the MFI would show values and dynamics less correlated with those of total annual precipitation.
The comparison between the spatial distribution of trends in annual precipitation MFI index shows the partial overlap of the areas affected by significant decreases (Figg. 6-7) in the provinces of Chieti and Pescara. In this large area the number of stations characterized by a significant drop in the index MFI is lower than the number of stations affected by significant decrease of rainfall. The significant reduction of the index MFI is particularly relevant in the north of the province of Teramo and in a central belt that covers the provinces of Aquila and Pescara. In the provinces of Pescara and Chieti the same phenomenon affects few locations of the coastal hilly area.

CONCLUSIONS

The use of the Index MFI has allowed us to analyze the climatic aggressiveness of rainfall in the Abruzzo region. Despite of its simplicity, the MFI index showed a good agreement with the RUSLE aggressivity factor R, computed at some stations of the region with reference to a limited period of time.
The analysis of the spatial variability of the MFI, showed that, due to the climatic characteristics of the region, MFI is usually higher in areas with higher annual rainfall. A general decrease in MFI, usually linked to the decline in annual rainfall, was also observed. Overall, this significant decrease affects much more the internal areas than the hilly coast.

REFERENCES

Arnoldus H.M.J., 1980. *An approximation of the rainfall factor in the Universal SoilLoss Equation. In Assessment of erosion* - FAO Land and Water Devel. Div. – Wiley & Sons, England, 127-132.
Andersson T., 1981. *Bergeron and the oreigenic maxima of precipitation*, in Weather and weather maps, edited by G.H. Liljequist, Birkhauser, 559-576.
Deyanira L.L., Donald G., 2005. *Assessing the rain erosivity and rain distribution in different agro-*

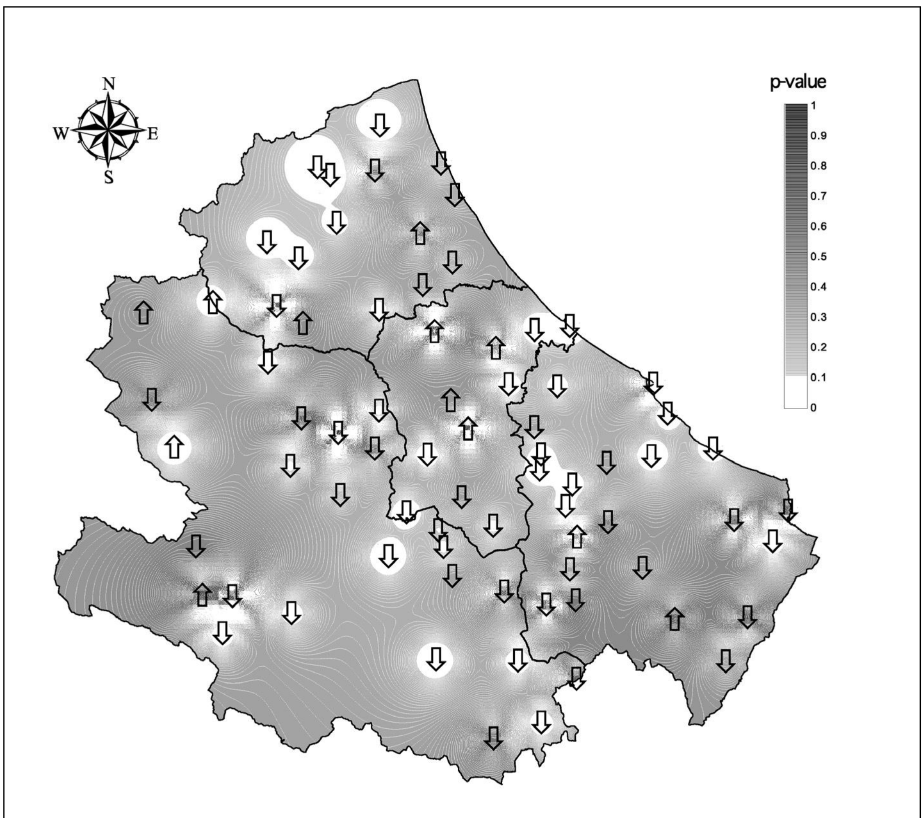

Fig. 6 - Spatial distribution of cumulative annual precipitation trend. The areas colored in white are those where significant trends occur (p-value <0.10). The arrows down indicate a significant decreasing trends while the arrows to the top ones indicates a significant increasing trend.
Fig. 6 - Distribuzione spaziale dei trend delle precipitazioni cumulate annue. Le aree colorate di bianco sono quelle dove si verificano trend significativi (p-value <0.10). Le frecce verso il basso indicano trend decrescenti, mentre quelle verso l'alto indicano trend crescenti.

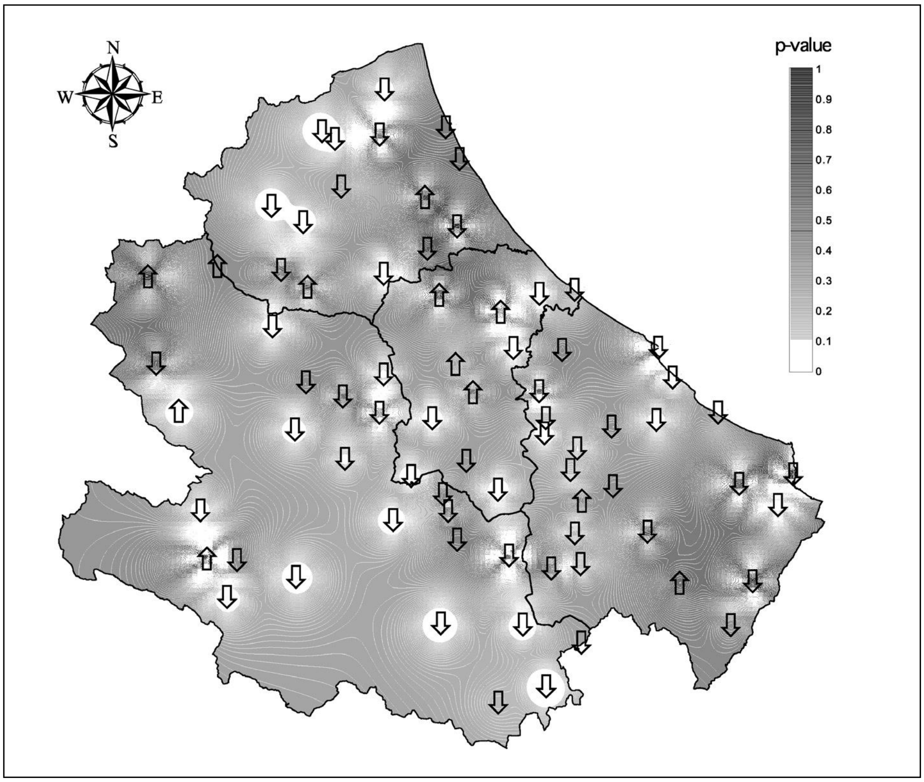

Fig. 7 - Spatial distribution of the MFI index trend. The areas colored in white are those where significant trends occur (p-value <0.10). The arrows down indicate a significant decreasing trends while the arrows to the top ones indicates a significant increasing trend.
Fig. 7 - Distribuzione spaziale dei trend dell'indice MFI. Le aree colorate di bianco sono quelle dove si verificano trend significativi (p-value <0.10). Le frecce verso il basso indicano trend decrescenti, mentre quelle verso l'alto indicano trend crescenti.

climatological zones in Venezuela. Sociedade & Natureza, Uberlândia, Special Issue, 16-29.

Bagarello V., D'Asaro F., 1994. *Estimating single storm erosion index.* Trans. ASAE, 37(3): 785-791.

Brown L.C., Foster G.R., 1987. *Storm erosivity using idealized intensity distributions*. Trans. ASAE, 30, 379-386.

CORINE 1995. *Soil erosion risk and important land resources in the southern regions of the European Community*. EUR 13233 EN.

Coutinho M.A., Tomas P.P., 1994. *Comparison of Fournier with Wischmeier rainfall erosivity indices*. In: Rickson, R.J. (Ed.). Conserving Soil Resources, European Perspectives. CAB International, Wallingford.

De Luis M., Gonzalez-Hidalgo., Longares L.A. 2010. *Is rainfall erosivity increasing in the mediterranean iberian peninsula?.* Land Degradation & Development 21:139-144.

Di Lena B., Antenucci F., Mariani L., 2012. *Space and time evolution of the Abruzzo precipitation*, Italian Journal of Agrometeorology, n.1/2012, 5-20.

Ferro V., Giordano G., Iovino M., 1991. *Isoerosivity and erosion risk map for Sicily*, Hydrological Sciences, Journal des Sciences Hydrologiques, 36, 6, 12.

Fournier F. 1960. *Climat et Erosion*. PUF: Paris.

Gregori E., Andrenelli M.C., ZORN G., 2006. *Assessment and classification of climatic aggressivenes with renard to slope instability phenomena connected to hidrological and morphological processes.* Journal of Hydrology 329, 489-499.

Kendall M.G., 1975. *Rank Correlation Measures*. Charles Griffin, London, 1975.

Lo A., El-Swaify S.A., Dangler E.W., Shinshiro L., 1985. *Effectiveness of EI30 as erosivity index in Hawaii. In El-Swaify, Moldenhauer, Lo (Editors).* Soil Con. Soc. Amer., Ankeny, 384-392.

Mann H.B., 1945. *Nonparametric tests against trend*. Econometrica. 13, pp. 245-259.

Oliver J.E., 1980. *Monthly precipitation distribution: A comparative index*. Professional Geographer 32: 300-309.

Renard K.G., Freimund J.R., 1994. *Using monthly precipitation data to estimate the R-factor in the revised USLE.* Journ. Of Hydr., 157: 287-306.

Renard K.G., Foster G.R., Weesies G.A., McCool D.K, and Yoder D.C., coordinators. 1997. *Predicting Soil Erosion by Water: A Guide to Conservation Planning with the Revised Soil Loss Equation (RUSLE)*. U.S. Dept. of Agriculture, Agric. Handbook No. 703, 404 pp.

Sen P.K. 1968. *Estimates of the regeression coefficient based Kendall's tau.* Journal of the American Statistical Association. 63, 1379-1389.

Taguas E. V., Carpintero E., Ayuso J.L., 2011. *Assessing land degradation risk through the long-term analysis of erosivity: a case study in southern Spain.* Land Degradation & Development DOI: 10.1002/ldr.1119.

Theil H., 1950. *A rank-invariant method for linear and polynomial regression analysis, I,II,III.* Nederlanndse Akademie wetwnschappen. 53, pp. 386-392, 521-525, 1397-1412.

Vergni L., Todisco F., Mannocchi F., 2009. *Evoluzione spazio-temporale delle precipitazioni e di alcuni indicatori di siccità in Umbria.* Atti IX Convegno nazioanle dell'Associazione Italiana di Ingegneria Agraria. Ischia Porto, 12-16 settembre 2009.

Wei T.C., McGuinnes L., 1973. *Reciprocal distances squared method: a computer technique for estimating areal precipitation.* U.S. Department of Agriculture, ARS-NS-8, pp. 1-23.

Wischmeier WH. 1959. *A rainfall erosion index from Universal Soil Loss Equation*. Soil Science Society of American Journal 24: 323-326.

Wiscmeier W.H., Smith D.D., 1978. *Predicting rainfall-erosion losses – A guide to conservation farming.* U.S. Dept. of Agric., Agr. Handbook n. 537.